J Sci Comput
DOI 10.1007/s10915-012-9642-3

A Non-oscillatory Central Scheme for One-Dimensional Two-Layer Shallow Water Flows along Channels with Varying Width

Jorge Balbás · Smadar Karni

Received: 9 January 2012 / Revised: 28 August 2012 / Accepted: 31 August 2012

Abstract We present a new high-resolution, non-oscillatory semi-discrete central scheme for one-dimensional two-layer shallow-water flows along channels with non-uniform rectangular cross sections and bottom topography. The scheme extends existing central semi-discrete schemes for hyperbolic conservation laws and it enjoys two properties crucial for the accurate simulation of shallow-water flows: it preserves the positivity of the water height, and it is well balanced, i.e., the source terms arising from the geometry of the channel are discretized so as to balance the non-linear hyperbolic flux gradients. Along with a detailed description of the scheme and proofs of these two properties, we present several numerical experiments that demonstrate the robustness of the numerical algorithm.

Keywords Hyperbolic systems of conservation and balance laws · Semi-discrete schemes · Saint-Venant system of shallow-water equations · Non-oscillatory reconstructions · Channels with irregular geometry

1 Introduction

1.1 The Balance Law

In this paper we present a second-order accurate, non-oscillatory semi-discrete central scheme for one-dimensional, two-layer shallow-water flows along channels with non-uniform rectangular cross sections and bottom topography. For nearly horizontal flows, the *depth average* of Euler equations results in the *balance law*, [1, 7]

$$\frac{\partial A_1}{\partial t} + \frac{\partial Q_1}{\partial x} = 0, \tag{1a}$$

J. Balbás (✉)
Department of Mathematics, California State University, Northridge, CA 91330, USA
e-mail: jorge.balbas@csun.edu

S. Karni
Department of Mathematics, University of Michigan, Ann Arbor, MI 48109, USA
e-mail: karni@umich.edu

Published online: 14 September 2012

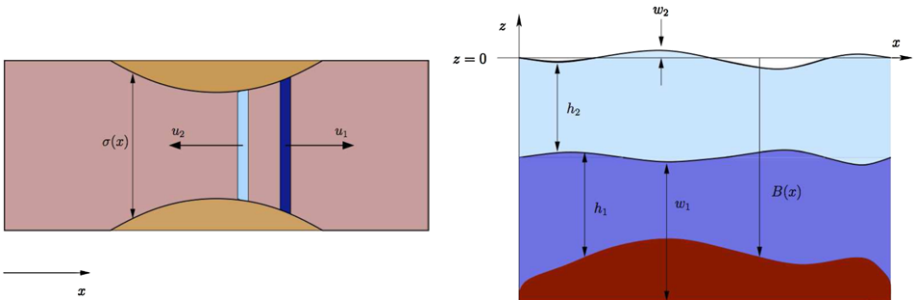

Fig. 1 *Left*: overview of a channel with a parabolic contraction. *Right*: flow profile for a flow described by system (1a)–(1d)

$$\frac{\partial Q_1}{\partial t} + \frac{\partial}{\partial x}\left(\frac{Q_1^2}{A_1} + \frac{1}{2}g\sigma h_1^2 + rg\sigma h_1 h_2\right) = \left(\frac{1}{2}gh_1^2 + rgh_1h_2\right)\sigma' - g\sigma h_1 B' + rg\sigma h_2 \frac{\partial h_1}{\partial x}, \tag{1b}$$

$$\frac{\partial A_2}{\partial t} + \frac{\partial Q_2}{\partial x} = 0, \tag{1c}$$

$$\frac{\partial Q_2}{\partial t} + \frac{\partial}{\partial x}\left(\frac{Q_2^2}{A_2} + \frac{1}{2}g\sigma h_2^2\right) = \frac{1}{2}g\sigma' h_2^2 - g\sigma h_2 B' - g\sigma h_2 \frac{\partial h_1}{\partial x}, \tag{1d}$$

where A_i, h_i, and $\sigma(x)$ stand, respectively, for the *wet* cross-section of each layer, the thickness of layer i ($i = 1, 2$ representing, respectively, the lower and upper layers), and the channel breadth, i.e., $A_i = \sigma h_i$, Q_i is the *discharge*, i.e., $Q_i = A_i u_i$, with u_i denoting the fluid velocity of layer i, $B(x)$ describes the bottom topography of the channel, g is the acceleration of gravity, and, $r = \dfrac{\rho_2}{\rho_1} \approx 1$, is the ratio of the fluid densities (see Fig. 1). The geometry of the channel, given by $\sigma(x)$ and $B(x)$, need not to be continuous.

1.2 Properties of the System

The non-conservative terms on the right hand side of the balance law (1a)–(1d) prevent us from writing the system in conservation form, yet these terms need to be taken into account when determining the underlying characteristic structure of the system. In order to find its characteristic decomposition, we write the system in the form,

$$\frac{\partial v}{\partial t} + \frac{\partial}{\partial x} f(v) = S_1\big(v, \sigma, \sigma', B'\big) + S_2(v, v_x, \sigma) \tag{2}$$

where $S_2(v_x) = (0, rg\sigma h_2 \frac{\partial h_1}{\partial x}, 0, -g\sigma h_2 \frac{\partial h_1}{\partial x})^\top$ holds the non-conservative products of $\dfrac{\partial h_1}{\partial x}$ and $S_1(v, \sigma, \sigma', B')$ the remaining *geometric* source terms.

This allows us to write the system in non-conservative quasilinear form

$$\frac{\partial v}{\partial t} + A\frac{\partial v}{\partial x} = \widetilde{S}_1(x, v) \tag{3}$$

where A stands for the *modified Jacobian*,

$$A = \frac{df}{dv} - \begin{pmatrix} 0 & 0 & 0 & 0 \\ rgh_2 & 0 & 0 & 0 \\ 0 & 0 & 0 & 0 \\ -gh_2 & 0 & 0 & 0 \end{pmatrix} = \begin{pmatrix} 0 & 1 & 0 & 0 \\ gh_1 - u_1^2 & 2u_1 & rgh_1 & 0 \\ 0 & 0 & 0 & 1 \\ gh_2 & 0 & gh_2 - u_2^2 & 2u_2 \end{pmatrix}. \tag{4}$$

The eigen values of this modified Jacobian are given by the roots of the characteristic polynomial

$$\left(\lambda^2 - 2u_1\lambda + u_1^2 - gh_1\right)\left(\lambda^2 - 2u_2\lambda + u_2^2 - gh_2\right) = rgh_1h_2, \tag{5}$$

which cannot be computed explicitly. For the most part, however, we are concerned with flows such that $r \sim 1$ and $u_1 \sim u_2$ (e.g., oceanic flows), in which case, a first order expansion in the terms $1 - r$ and $u_1 - u_2$, yields the approximations, [2]

$$\lambda_{1,2} \approx u_m \pm \sqrt{g(h_1 + h_2)}, \tag{6a}$$

$$\lambda_{3,4} \approx u_c \pm \sqrt{(1-r)g\frac{h_1h_2}{h_1 + h_2}\left(1 - \frac{(u_1 - u_2)^2}{(1-r)g(h_1 + h_2)}\right)}, \tag{6b}$$

where

$$u_m = \frac{h_1u_1 + h_2u_2}{h_1 + h_2} \quad \text{and} \quad u_c = \frac{h_1u_2 + h_2u_1}{h_1 + h_2}. \tag{7}$$

This indicates that the system may loose hyperbolicity if the condition

$$(u_1 - u_2)^2 \le (1 - r)g(h_1 + h_2) \tag{8}$$

We note that this condition is not strict since (8) is only approximate.

The system (1a)–(1d) is endowed with the entropy function

$$\mathcal{E}(x,t) = \sigma\left[\rho_1h_1\left(\frac{1}{2}u_1^2 + \frac{1}{2}gh_1\right) + \rho_2h_2\left(\frac{1}{2}u_2^2 + \frac{1}{2}gh_2 + gh_1\right)\right], \tag{9}$$

and satisfies the entropy inequality

$$\frac{\partial\mathcal{E}}{\partial t} + \frac{\partial}{\partial x}\left[\rho_1h_1u_1\left(\frac{1}{2}u_1^2 + gh_1 + rgh_2\right) + \rho_2h_2u_2\left(\frac{1}{2}u_2^2 + gh_2 + gh_1\right)\right] \le 0. \tag{10}$$

Smooth steady-state solutions of (1a)–(1d) satisfy

$$Q_i = \sigma h_iu_i = \text{Const.}, \quad i = 1, 2, \tag{11a}$$

$$E_1 = \frac{1}{2}u_1^2 + g(h_1 + rh_2 + B) = \text{Const.}, \tag{11b}$$

$$E_2 = \frac{1}{2}u_2^2 + g(h_1 + h_2 + B) = \text{Const.}, \tag{11c}$$

where, for example, one readily recognizes the trivial steady-state of rest

$$\begin{aligned} &u_i(x) = 0 \ (i = 1, 2), \\ &w_1(x) = h_1(x) + B(x) = \text{Const.}, \quad \text{and} \quad w_2(x) = w_1(x) + h_2(x) = \text{Const.} \end{aligned} \tag{12}$$

The parameters Q_i and E_i (together with the topography $B(x)$ and channel geometry $\sigma(x)$) determine the steady-state solution as the root of the nonlinear system of (12), [1–3, 8, 21, 27]. To this end, it is convenient to define the internal Froude number of each layer,

$$F_i^2 = \frac{u_i^2}{g' h_i}, \quad i = 1, 2, \tag{13}$$

where $g' = (1 - r)g$ stands for the reduced gravity, and the composite Froude number,

$$G^2 = F_1^2 + F_2^2. \tag{14}$$

These dimensionless quantities describe the essential non-linearity of the flow, flows with composite Froude number $G^2 < 1$ are said to be subcritical or *fluvial*, and flows with Froude number $G^2 > 1$ supercritical or *torrential*. The interplay between the breath of the channel, $\sigma(x)$, and the topography, $B(x)$, controls the flow. For example, if the crest of the topography ($B'(x) = 0$) and the throat of the channel ($\sigma'(x) = 0$) occur at the same point, then at that point either the solution is symmetric, $(h_i)_x = 0$, or the flow reaches criticality $G^2 = 1$. Channel geometries where the crest and throat occur at different points lead to more complex flow profiles. In some cases, the flow will reach criticality at a point located between the crest of the channel's floor and its throat, and in cases where the crest and the throat are relatively far apart from each other, critical points may occur at either of those two locations or even at both [1–3, 8, 21, 27].

1.3 Numerical Simulation of Two-Layer Shallow-Water Flows

The system admits discontinuous solutions and requires robust numerical schemes that are suitable for calculating discontinuous flows. For such flows, the nonconservative products may be large relative to the geometric source terms and render the solution very sensitive to the details of their discretization and introduce spurious oscillations in the approximate solutions.

Changes in the solution of (1a)–(1d) in time arise when flux gradients are out of balance with the source terms. The simulation of *near* steady-state flows require numerical schemes capable of recognizing such balance. In [13] it is shown that numerical schemes that are able to recognize and respect the balance between flux gradients and source terms often give superior results when computing such near steady-state flows, whereas non-oscillatory schemes that simply employ a high-order discretization of source terms without regard for balance may trigger the onset of oscillations –possibly larger than the small perturbations, and fail to capture steady-states. Perfectly recognizing such balance may not always be possible, and schemes that respect steady-state solutions either exactly or to the order of the numerical approximation are commonly called 'well-balanced', [1, 4, 13, 15, 16, 24, 26].

Another challenge arises when computing solutions where $h_1 \to 0$ (e.g., internal dam break) and/or $h_2 \to 0$. In such cases, the truncation error of the numerical scheme may cause the depth of either layer, h_1 or h_2, to become negative, causing the computation to fail. Positivity preserving schemes have the desirable property that if the data has positive

(non-negative) depth, so does the numerical solution. Positivity preserving schemes enjoy enhanced stability near dry states.

In this paper, we introduce a semi-discrete central scheme for calculating flows described by (1a)–(1d). The scheme is second order accurate, well-balanced and positivity preserving. Nonoscillatory schemes based on central differencing offer a robust, yet simple, approach for computing the discontinuous solutions of hyperbolic problems, see for example [5, 6, 12, 17, 20, 22]. Several central schemes have been extended to handle systems with geometric source terms. In [24] Russo introduces a fully-discrete, well balance central scheme for flows along channels of constant width, and in [13, 15] several semi-discrete central schemes for one- and two-dimensional shallow-water flows are presented. The central scheme described in this work extends the work in [13, 15, 16, 23] to flows in variable geometry. The numerical solutions of two-layer flows along channels with arbitrary geometry have been addressed in [7], where an Q-scheme for a hyperbolic system similar to the balance law (1a)–(1d) is proposed, and in [26] where single-layer flows along channels with arbitrary geometries are simulated with an upwind scheme.

The proposed scheme is described in Sect. 2, and it's established to preserve the positivity of water height of the bottom layer and to be well-balanced. Numerical solutions are presented in Sect. 3 for a variety of flow regimes, demonstrating the scheme's accuracy and robustness and demonstrating its ability to simulate a wide range of flows.

2 A Central Scheme for One-Dimensional Two-Layer Shallow-Water Flows

In this section we construct a central scheme for the accurate simulation of two-layer shallow-water flows described by the balance law (1a)–(1d). In particular, we seek a scheme that is positivity preserving and well-balanced. The scheme extends previous works in [4, 13, 15, 16] to two-layer flows in variable geometry. This extension is not trivial; the non-conservative products require special treatment so as to guarantee stability. And the varying width of the channel makes balancing more difficult; while in the constant channel width model ($\sigma \equiv 1$), well-balancing may be accomplished solely by choosing an appropriate discretization of the source term, in the variable geometry case, the conserved variables $A_i = \sigma h_i$ and $Q_i = \sigma h_i u_i$ depend on the geometry σ, which renders steady-state preservation and positivity more strongly coupled with, for example, the polynomial reconstruction of the conserved variables.

Following [16], we reformulate (1a)–(1d) in terms of the total elevation of the bottom layer, $w_1 = h_1 + B$ and its total area, $A_1^T = A_1 + \sigma B = \sigma w_1$; we also add the term $(g\sigma(\frac{1}{2}h_1 + B)h_1)_x$ to both sides of (1b), and $(g\sigma(\frac{1}{2}h_2 + h_1 + B)h_2)_x$ to both sides of (1d). These linear transformation leads the equivalent formulation

$$\frac{\partial A_1^T}{\partial t} + \frac{\partial Q_1}{\partial x} = 0 \tag{15a}$$

$$\frac{\partial Q_1}{\partial t} + \frac{\partial}{\partial x}\left(\frac{Q_1^2}{A_1} + g\sigma \widehat{w}_2 h_1\right) = g\widehat{w}_2 h_1 \sigma' + g\sigma \widehat{w}_2 \frac{\partial h_1}{\partial x} \tag{15b}$$

$$\frac{\partial A_2}{\partial t} + \frac{\partial Q_2}{\partial x} = 0 \tag{15c}$$

$$\frac{\partial Q_2}{\partial t} + \frac{\partial}{\partial x}\left(\frac{Q_2^2}{A_2} + g\sigma w_2 h_2\right) = g w_2 h_2 \sigma' + g\sigma w_2 \frac{\partial h_2}{\partial x} \tag{15d}$$

where $w_2 = h_2 + w_1$ and $\widehat{w}_2 = r h_2 + w_1$.

This formulation preserves weak solutions allows the numerical scheme to detect changes (or the lack of them) in the total water elevation of the bottom layer, w_1, which in turn, facilitates ensuring the preservation of steady-states of rest. Furthermore, the non-conservative source terms are scaled to $\mathcal{O}(w_2)$, so that when the total water elevation is measured as the displacement from the water surface at rest (see Fig. 1), these terms are small and do not affect the stability of the scheme.

2.1 Semi-Discrete Central Formulation

We begin by describing the semi-discrete central scheme framework for approximating solutions for hyperbolic conservation laws (consult [14] and [17] for further details),

$$v_t + f(v)_x = 0. \tag{16}$$

For a fixed spatial scale Δx, we consider the partition of the solution domain into the grid cells $I_j := [x_j - \Delta x/2, x_j + \Delta x/2]$, and denote by $\overline{v}_j(t)$the cell average of $v(x,t)$ over the cell I_j,

$$\overline{v}_j(t) = \frac{1}{\Delta x}\int_{x_{j-\frac{1}{2}}}^{x_{j+\frac{1}{2}}} v(x,t)dx.$$

Integrating (16) over each I_j results in the equivalent semi-discrete formulation

$$\frac{d}{dt}\overline{v}_j(t) = -\frac{1}{\Delta x}\Big(f\big(v(x_{j+\frac{1}{2}},t)\big) - f\big(v(x_{j-\frac{1}{2}},t)\big)\Big). \tag{17}$$

Equation (17) is approximated by the collection of (semi-discrete) ODEs:

$$\frac{d}{dt}\overline{v}_j(t) = -\frac{H_{j+\frac{1}{2}}(t) - H_{j-\frac{1}{2}}(t)}{\Delta x}, \tag{18}$$

where the flux at cell interfaces, $f(v(x_{j\pm\frac{1}{2}},t))$, is approximated by the numerical flux $H_{j\pm\frac{1}{2}}(t)$ given by

$$H_{j\pm\frac{1}{2}}(t) = \frac{f(v^+_{j\pm\frac{1}{2}}(t)) + f(v^-_{j\pm\frac{1}{2}}(t))}{2} - \frac{a_{j\pm\frac{1}{2}}}{2}\big(v^+_{j\pm\frac{1}{2}}(t) - v^-_{j\pm\frac{1}{2}}(t)\big). \tag{19}$$

Here, the interface point-values of the solution, $v^{\pm}_{j\pm\frac{1}{2}}(t)$, are recovered from the cell averages $\{\overline{v}_j(t)\}$ via a non-oscillatory polynomial reconstruction $v(x,t) \approx R(x;t) = \sum_j p_j(x;t)\cdot \mathbf{1}_{I_j}$, i.e.,

$$v^-_{j+\frac{1}{2}} := p_j(x_{j+\frac{1}{2}}) \quad \text{and} \quad v^+_{j+\frac{1}{2}} := p_{j+1}(x_{j+\frac{1}{2}}), \tag{20}$$

(consult Sect. 2.2.1 for the definition of the polynomials $p_j(x)$) and $a_{j+\frac{1}{2}}$ stands for (an estimate of) the maximum wave speed of the conservation law, (16), at the cell interface $x_{j+\frac{1}{2}}$, given by the spectral radius of the Jacobian matrix of $f(v)$, $\partial f/\partial v$. The zero order reconstruction reproduces the well-known LxF scheme [18].

This semi-discrete formulation, (18), and its central-upwind sequel, [14], provide a general framework for non-oscillatory central schemes, requiring for their actual implementation two ingredients: (i) a non-oscillatory polynomial reconstruction of the interface values

$\{v^{\pm}_{j\pm\frac{1}{2}}\}_j$ from their cell averages $\{\overline{v}_j(t)\}_j$, and (ii) an evolution routine (i.e., an ODE solver) to update these cell averages according to (18).

In analogy, the semi-discrete formulation for the balance law

$$v_t + f(v)_x = S(v, v_x, x), \tag{21}$$

yields the semi-discrete system

$$\frac{d}{dt}\overline{v}_j(t) = -\frac{H_{j+\frac{1}{2}}(t) - H_{j-\frac{1}{2}}(t)}{\Delta x} + \overline{S}_j\big(v, v_x, \sigma, \sigma'\big) \tag{22}$$

where the numerical fluxes, $H_{j\pm\frac{1}{2}}$, are given by (19), and the cell average of the source term, $\overline{S}_j$, amounts to (see Appendix B for details)

$$\overline{S}_j\big(v, v_x, \sigma, \sigma'\big) = \frac{1}{\Delta x}\Bigg[\frac{1}{2}\int_{x^-_{j-\frac{1}{2}}}^{x^+_{j-\frac{1}{2}}} S\big(v, v_x, \sigma, \sigma'\big)dx + \int_{x^+_{j-\frac{1}{2}}}^{x^-_{j+\frac{1}{2}}} S\big(v, v_x, \sigma, \sigma'\big)dx$$

$$+ \frac{1}{2}\int_{x^-_{j+\frac{1}{2}}}^{x^+_{j+\frac{1}{2}}} S\big(v, v_x, \sigma, \sigma'\big)dx\Bigg]. \tag{23}$$

For the two-layer shallow-water system, (15a)–(15d),

$$v = \begin{pmatrix} A_1^T \\ Q_1 \\ A_2 \\ Q_2 \end{pmatrix} = \begin{pmatrix} \sigma w_1 \\ \sigma h_1 u_1 \\ \sigma h_2 \\ \sigma h_2 u_2 \end{pmatrix}, \qquad f(v) = \begin{pmatrix} \sigma h_1 u_1 \\ \sigma h_1 u_1^2 + g\sigma \widehat{w}_2 h_1 \\ \sigma h_2 u_2 \\ \sigma h_2 u_2^2 + g\sigma w_2 h_2 \end{pmatrix}, \tag{24}$$

and

$$S\big(v, v_x, \sigma, \sigma'\big) = \begin{pmatrix} 0 \\ g(\widehat{w}_2 h_1 \sigma' + \sigma \widehat{w}_2 \frac{\partial h_1}{\partial x}) \\ 0 \\ g(w_2 h_2 \sigma' + \sigma w_2 \frac{\partial h_2}{\partial x}) \end{pmatrix}. \tag{25}$$

In addition to the non-oscillatory polynomial reconstruction and the evolution routine needed for the implementation of (18), the approximation of balance laws requires a suitable discretization of the integral of the source term in (23).

2.2 Non-oscillatory Second-Order Reconstruction

In order to recover the interface values $v^{\pm}_{j\pm\frac{1}{2}}(t)$ in (19) from the cell averages $\overline{v}_j(t)$, we employ a piece-wise linear reconstruction,

$$v(x,t) = R\big(x; \overline{v}(t)\big) := \sum_j p_j(x). \tag{26}$$

This reconstruction procedure is at the heart of high-resolution non-oscillatory central schemes, and requires the coefficients of the polynomials $\{p_j(x)\}$ to be determined so that $R(x; \overline{v}(t))$ satisfies the following three essential properties:

– $\mathcal{P}_1$—Conservation of cell averages: $\overline{p}_j(x) = \overline{v}_j(t)$.
– $\mathcal{P}_2$—Accuracy: $R(x;\overline{v}(t)) = v(x,t) + \mathcal{O}((\Delta x)^2)$ (in smooth regions).
– $\mathcal{P}_3$—Non-oscillatory behavior of $\sum_j p_j(x)$.

For the shallow-water system (15a)–(15d) we also require that the reconstructed values of the total area of the bottom layer, A_1^T, the wet area of the second layer, A_2, and the corresponding values of their total height, w_1 and h_2, satisfy the following properties:

– $\mathcal{P}_4$—Flux gradient and source balancing: for steady-sates of rest, the interface values of the water heights, w_1 and h_2, must be reconstructed so as to satisfy

$$w^{\pm}_{1,j+\frac{1}{2}} = \text{Const.}, \qquad w^{\pm}_{2,j+\frac{1}{2}} = \text{Const.} \quad \text{and} \quad \widehat{w}^{\pm}_{2,j+\frac{1}{2}} = \text{Const.} \tag{27}$$

– $\mathcal{P}_5$—Positivity: the reconstructed values of $w^{\pm}_{1,j\pm\frac{1}{2}}(t)$ and $h^{\pm}_{2,j\pm\frac{1}{2}}(t)$ must yield $h^{\pm}_{i,j\pm\frac{1}{2}}(t) \geq 0$, so as to ensure the positivity of $\overline{h}_{i,j}(t+\Delta t)$ $(i = 1, 2)$.

We note that properties $\mathcal{P}_4$ and $\mathcal{P}_5$, tie the channel's geometry to the flow variables (i.e., $A_1^T = \sigma(h_1 + B)$ and $A_2 = \sigma h_2$), and, thus, require the bottom topography and channel's width to be discretized so that the interface values of w_1 and h_2 are consistent with the corresponding areas, A_1^T and A_2. To this end, we evaluate the bottom topography and the channel's breath to the left/right of the cell interfaces $x_{j+\frac{1}{2}}$, denoting the corresponding values by the superscripts $-$ and $+$, that is,

$$\sigma^{\pm}_{j+\frac{1}{2}} := \sigma\big(x^{\pm}_{j+\frac{1}{2}}\big) \quad \text{and} \quad B^{\pm}_{j+\frac{1}{2}} := B\big(x^{\pm}_{j+\frac{1}{2}}\big). \tag{28}$$

This allows us to consider discontinuous bathimetry data from which we can define the averages and differences

$$\overline{B}_j = \frac{1}{2}\big(B^{+}_{j-\frac{1}{2}} + B^{-}_{j+\frac{1}{2}}\big) \quad \text{and} \quad \Delta B_j = \frac{B^{-}_{j+\frac{1}{2}} - B^{+}_{j-\frac{1}{2}}}{\Delta x}, \tag{29}$$

for the bottom, and

$$\overline{\sigma}_j = \frac{1}{2}\big(\sigma^{+}_{j-\frac{1}{2}} + \sigma^{-}_{j+\frac{1}{2}}\big) \quad \text{and} \quad \Delta\sigma_j = \frac{\sigma^{-}_{j+\frac{1}{2}} - \sigma^{+}_{j-\frac{1}{2}}}{\Delta x}, \tag{30}$$

for the width. Which in turn allow us to approximate the channel's bottom and walls, respectively, with the piecewise linear reconstructions

$$B(x) = \overline{B}_j + \Delta B_j(x - x_j), \quad \text{and} \quad \sigma(x) = \overline{\sigma}_j + \Delta\sigma_j(x - x_j) \quad \text{for } x_{j-\frac{1}{2}} < x < x_{j+\frac{1}{2}}, \tag{31}$$

a choice that also guaranties properties $\mathcal{P}_1$–$\mathcal{P}_3$ for the geometry and is consistent with the second order accuracy sought for the scheme.

2.2.1 Minmod Reconstruction: Properties $\mathcal{P}_1$–$\mathcal{P}_3$

To guarantee properties $\mathcal{P}_1$–$\mathcal{P}_3$, we employ a second-order *minmod* reconstruction, [10, 19]. The total area of the bottom layer, A_1^T, the wet area of the top layer, A_2, and both discharges, Q_i $(i = 1, 2)$, are reconstructed from their cell averages as the piecewise

linear functions (the reconstruction is applied to values at time t, thus we can avoid the explicit reference to the time variable for its description)

$$p_j(x) = \overline{v}_j + v'_j(x - x_j), \tag{32}$$

with the slopes v'_j calculated as

$$v'_j = \frac{1}{\Delta x}\text{minmod}(\alpha\Delta_-\overline{v}_j, \Delta_0\overline{v}_j, \alpha\Delta_+\overline{v}_j), \tag{33}$$

where $1 \le \alpha < 2$, and

$$\text{minmod}(x_1, x_2, x_3, \ldots, x_k) = \begin{cases} \min_j(x_j) & \text{if } x_j > 0 \quad \forall j, \\ \max_j(x_j) & \text{if } x_j < 0 \quad \forall j, \\ 0 & \text{otherwise.} \end{cases} \tag{34}$$

The choice of limiter (33) allows for sharper, less dissipative, reconstructions than the usual two argument minmod limiter corresponding to $\alpha = 1$. For the numerical examples presented in Sect. 3 the best results are obtained with the value $\alpha = 1.4$, a value that we determine empirically.

2.2.2 *Reconstruction of h_1 and h_2: Properties $\mathcal{P}_4$ and $\mathcal{P}_5$*

In order to produce a well-balanced positivity preserving scheme, we first recover the cell averages of w_1 and h_2 from those of A_1^T and A_2 respectively as

$$\overline{w}_{1,j} := \frac{\overline{A}^T_{1,j}}{\sigma_j}, \quad \text{and} \quad \overline{h}_{2,j} := \frac{A_{2,j}}{\sigma_j}. \tag{35}$$

For the flows calculated in Sect. 3 below, the initial conditions are given for u_i (or Q_i, $i = 1, 2$), w_1, and h_2, allowing us to initialize $\overline{A}^T_{1,j} := \overline{\sigma}_j\overline{w}_{1,j}$ and $\overline{A}_{2,j} := \overline{\sigma}_j\overline{h}_{2,j}$ (other values can be chosen within the second order accuracy of the scheme. The interface values $w^{\mp}_{1,j\pm\frac{1}{2}}$ and $h^{\mp}_{2,j\pm\frac{1}{2}}$ are then obtained using the minmod reconstruction (32)–(34).

Clearly, these reconstructed values will remain constant if the corresponding cell averages $\overline{w}_{1,j}$ and $\overline{h}_{2,j}$ are constant for all j, and so will be the total flow depths $w^{\mp}_{2,j\pm\frac{1}{2}}$ and $\widehat{w}^{\mp}_{2,j\pm\frac{1}{2}}$, as needed to preserve steady-states of rest.

To ensure the positivity of $h^{\mp}_{1,j\pm\frac{1}{2}}$, we follow [15], and limit the slope of the reconstructed values of w_1 as follows (see Fig. 2):

$$\begin{aligned} &\text{if } w^+_{1,j-\frac{1}{2}} < B^+_{j-\frac{1}{2}}, \quad \text{then set} \quad w'_{1,j} := 2\big(\overline{w}_{1,j} - B^+_{j-\frac{1}{2}}\big), \\ &\Rightarrow \quad w^+_{1,j-\frac{1}{2}} = B^+_{j-\frac{1}{2}}, \quad \text{and} \quad w^-_{1,j+\frac{1}{2}} = \overline{w}_{1,j} + \frac{1}{2}w'_{1,j}, \end{aligned} \tag{36}$$

or

$$\begin{aligned} &\text{if } w^-_{1,j+\frac{1}{2}} < B^-_{j+\frac{1}{2}}, \quad \text{then set} \quad w'_{1,j} := 2\big(B^-_{j+\frac{1}{2}} - \overline{w}_{1,j}\big), \\ &\Rightarrow \quad w^-_{1,j+\frac{1}{2}} = B^-_{j+\frac{1}{2}}, \quad \text{and} \quad w^+_{1,j-\frac{1}{2}} = \overline{w}_{1,j} - \frac{1}{2}w'_{1,j}, \end{aligned} \tag{37}$$

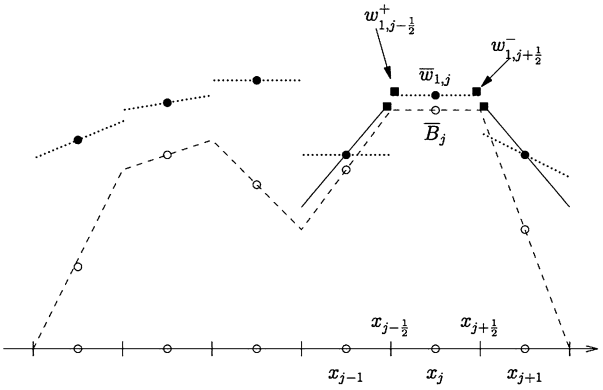

Fig. 2 Modified reconstruction of total water height of the bottom layer, w_1, over the piecewise linear approximation of bottom topography (*dashed line*). The minmod reconstruction is depicted by dotted lines over cell averages (*black dots*), the modified reconstruction is depicted by a *black solid line*, the interface pointvalues of w_1, $w_{1,j\pm\frac{1}{2}}$, are depicted by *black squares*

This linear reconstruction of w_1 clearly satisfies property $\mathcal{P}_5$ for h_1, $w^{\pm}_{1,j+\frac{1}{2}} \geq B^{\pm}_{j+\frac{1}{2}}$, which in turn will guarantee the positivity of $\overline{h}_{1,j}(t+\Delta t)$, whose interface values are defined as

$$\begin{aligned} h^-_{1,j+\frac{1}{2}} &:= w^-_{1,j+\frac{1}{2}} - B^-_{j+\frac{1}{2}} \\ h^+_{1,j-\frac{1}{2}} &:= w^+_{1,j-\frac{1}{2}} - B^+_{j-\frac{1}{2}}. \end{aligned} \tag{38}$$

To guarantee positivity of layer two, we follow a similar reconstruction for $w_2 = w_1 + h_2$, replacing w_1 with w_2, and B with w_1 in (36) and (37).

2.3 Regularization of Flow Velocities and Discharges for Thin Layers

The fluxes f in (24) require the pointwise values of the flow velocity $u^{\mp}_{i,j\pm\frac{1}{2}}$ $(i = 1, 2)$. Recovering the flow velocity via Q_i/A_i may be inaccurate when h_i (hence both Q_i and $A_i = \sigma h_i$) is very small, and may lead to instabilities. To prevent this, we follow the desingularization strategy proposed in [15], and compute the flow velocities, u_i, according to

$$u_i = \frac{\sqrt{2} A_i Q_i}{\sqrt{A_i^4 + \max(A_i^4, \epsilon)}}, \tag{39}$$

with $\epsilon = (\Delta x)^4$. When A_i is small, we must recalculate the discharge as $Q_i := A_i \cdot u_i$ so as to ensure the well balance and positivity properties (consult [15] for a detailed discussion of this and other desingularization techniques).

2.4 Balance: Discretization of the Source Term and Preservation of Steady-States

In the context of shallow-water flows, a useful guiding principle in the discretization of the source term in (1a)–(1d) and its cell average in (22) is that the resulting scheme is able to recognize and respect steady-state solutions. Analytically, such solutions are characterized by a perfect balance between the flux gradient and the source terms. Ideally, this property should be inherited by the scheme. In practice, however, a discrete perfect balance may not be possible to achieve for general steady-states, so we seek a discretization that perfectly respects steady-states of rest and settle for respecting general steady states to the order of the numerical approximation.

In order to achieve this balance between flux gradient and source terms, we calculate the numerical fluxes in (22) that result when steady-state of rest conditions ($u_i = 0, w_i = \text{Const.}, i = 1, 2$) are assumed, and seek a high-order discretization of the source term integrals that matches the numerical fluxes under these conditions. Under these steady-state conditions, the second and fourth components of the numerical flux $H_{j\pm\frac{1}{2}}$ reduce to

$$H^{Q_1}_{j+\frac{1}{2}}(t) = \frac{f^{Q_1}(v^-_{j+\frac{1}{2}}) + f^{Q_1}(v^+_{j+\frac{1}{2}})}{2} = \frac{g}{2}\big(\sigma^-_{j+\frac{1}{2}}\widehat{w}^-_{2,j+\frac{1}{2}}h^-_{1,j+\frac{1}{2}} + \sigma^+_{j+\frac{1}{2}}\widehat{w}^+_{2,j+\frac{1}{2}}h^+_{1,j+\frac{1}{2}}\big), \quad (40)$$

and

$$H^{Q_2}_{j+\frac{1}{2}}(t) = \frac{f^{Q_2}(v^-_{j+\frac{1}{2}}) + f^{Q_2}(v^+_{j+\frac{1}{2}})}{2} = \frac{g}{2}\big(\sigma^-_{j+\frac{1}{2}}w^-_{2,j\pm\frac{1}{2}}h^-_{2,j+\frac{1}{2}} + \sigma^+_{j+\frac{1}{2}}w^+_{2,j+\frac{1}{2}}h^+_{2,j+\frac{1}{2}}\big), \quad (41)$$

respectively. So that the corresponding flux difference terms in (22) read

$$\begin{aligned}-\frac{H^{Q_1}_{j+\frac{1}{2}}(t) - H^{Q_1}_{j-\frac{1}{2}}(t)}{\Delta x} = -\frac{g}{2\Delta x}\big(&\sigma^+_{j+\frac{1}{2}}\widehat{w}^+_{2,j+\frac{1}{2}}h^+_{1,j+\frac{1}{2}} + \sigma^-_{j+\frac{1}{2}}\widehat{w}^-_{2,j+\frac{1}{2}}h^-_{1,j+\frac{1}{2}}\\ &- \sigma^+_{j-\frac{1}{2}}\widehat{w}^+_{2,j-\frac{1}{2}}h^+_{1,j-\frac{1}{2}} - \sigma^-_{j-\frac{1}{2}}\widehat{w}^-_{2,j-\frac{1}{2}}h^-_{1,j-\frac{1}{2}}\big), \end{aligned} \quad (42)$$

and

$$\begin{aligned}-\frac{H^{Q_2}_{j+\frac{1}{2}}(t) - H^{Q_2}_{j-\frac{1}{2}}(t)}{\Delta x} = -\frac{g}{2\Delta x}\big(&\sigma^+_{j+\frac{1}{2}}w^+_{2,j+\frac{1}{2}}h^+_{2,j+\frac{1}{2}} + \sigma^-_{j+\frac{1}{2}}w^-_{2,j+\frac{1}{2}}h^-_{2,j+\frac{1}{2}}\\ &- \sigma^+_{j-\frac{1}{2}}w^+_{2,j-\frac{1}{2}}h^+_{2,j-\frac{1}{2}} - \sigma^-_{j-\frac{1}{2}}w^-_{2,j-\frac{1}{2}}h^-_{2,j-\frac{1}{2}}\big). \end{aligned} \quad (43)$$

Since these two components of the numerical flux are analogous, we focus, for brevity, on the first one of them, (42), and rewrite it as

$$\begin{aligned}-\frac{H^{Q_1}_{j+\frac{1}{2}}(t) - H^{Q_1}_{j-\frac{1}{2}}(t)}{\Delta x} = -\frac{g}{\Delta x}\Big[&\frac{1}{2}\big(\sigma^+_{j-\frac{1}{2}}\widehat{w}^+_{2,j-\frac{1}{2}}h^+_{1,j-\frac{1}{2}} - \sigma^-_{j-\frac{1}{2}}\widehat{w}^-_{2,j-\frac{1}{2}}h^-_{1,j-\frac{1}{2}}\big)\\ &+ \big(\sigma^-_{j+\frac{1}{2}}\widehat{w}^-_{2,j+\frac{1}{2}}h^-_{1,j+\frac{1}{2}} - \sigma^+_{j-\frac{1}{2}}\widehat{w}^+_{2,j-\frac{1}{2}}h^+_{1,j-\frac{1}{2}}\big)\\ &+ \frac{1}{2}\big(\sigma^+_{j-\frac{1}{2}}\widehat{w}^+_{2,j-\frac{1}{2}}h^+_{1,j-\frac{1}{2}} - \sigma^-_{j-\frac{1}{2}}\widehat{w}^-_{2,j-\frac{1}{2}}h^-_{1,j-\frac{1}{2}}\big)\Big] \end{aligned} \quad (44)$$

The first and third differences on the right of this equation represent, respectively, the jump of the flux, $f(v)$, across the left and right interfaces of the cell I_j, and the second, the net flux inside the cell. Denoting the positive terms in these differences by the superscript R and the negative ones by L, we can factor them into

$$\begin{aligned}\sigma^R\widehat{w}^R_2h^R_1 - \sigma^L\widehat{w}^L_2h^L_1 = &\frac{1}{4}\big(\sigma^R - \sigma^L\big)\big(\widehat{w}^R_2 + \widehat{w}^L_2\big)\big(h^R_1 + h^L_1\big)\\ &+ \frac{1}{4}\big(\sigma^R + \sigma^L\big)\big(\widehat{w}^R_2 + \widehat{w}^L_2\big)\big(h^R_1 - h^L_1\big)\end{aligned}$$

$$+\frac{1}{4}\left(\sigma^R-\sigma^L\right)\left(\widehat{w}_2^R-\widehat{w}_2^L\right)\left(h_1^R+h_1^L\right)$$
$$+\frac{1}{4}\left(\sigma^R+\sigma^L\right)\left(\widehat{w}_2^R-\widehat{w}_2^L\right)\left(h_1^R-h_1^L\right). \tag{45}$$

And noting that the minmod reconstruction (32)–(34) of w_1 and h_2 will ensure that the interface values $w^{\mp}_{2,j\pm\frac{1}{2}}$ and $\widehat{w}^{\mp}_{2,j\pm\frac{1}{2}}$ remain constant for all j for the steady-state of rest, and therefore, their differences in (44) (and the corresponding numerical flux of Q_2) will vanish (second line of (45)), the interface jumps reduce to

$$\begin{aligned}
&\sigma^+_{j\pm\frac{1}{2}}\widehat{w}^+_{2,j\pm\frac{1}{2}}h^+_{1,j\pm\frac{1}{2}}-\sigma^-_{j\pm\frac{1}{2}}\widehat{w}^-_{2,j\pm\frac{1}{2}}h^-_{1,j\pm\frac{1}{2}}\\
&\quad=\frac{1}{4}\left(\widehat{w}^+_{2,j\pm\frac{1}{2}}+\widehat{w}^-_{2,j\pm\frac{1}{2}}\right)\left[\left(\sigma^+_{j\pm\frac{1}{2}}-\sigma^-_{j\pm\frac{1}{2}}\right)\left(h^+_{1,j\pm\frac{1}{2}}+h^-_{1,j\pm\frac{1}{2}}\right)\right.\\
&\qquad\left.+\left(\sigma^+_{j\pm\frac{1}{2}}+\sigma^-_{j\pm\frac{1}{2}}\right)\left(h^+_{1,j\pm\frac{1}{2}}-h^-_{1,j\pm\frac{1}{2}}\right)\right],
\end{aligned}\tag{46}$$

and the net flux within the cell to

$$\begin{aligned}
&\sigma^-_{j+\frac{1}{2}}\widehat{w}^-_{2,j+\frac{1}{2}}h^-_{1,j+\frac{1}{2}}-\sigma^+_{j-\frac{1}{2}}\widehat{w}^+_{2,j-\frac{1}{2}}h^+_{1,j-\frac{1}{2}}\\
&\quad=\frac{1}{4}\left(\widehat{w}^-_{2,j+\frac{1}{2}}+\widehat{w}^+_{2,j-\frac{1}{2}}\right)\left[\left(\sigma^-_{j+\frac{1}{2}}-\sigma^+_{j-\frac{1}{2}}\right)\left(h^-_{1,j+\frac{1}{2}}+h^+_{1,j-\frac{1}{2}}\right)\right.\\
&\qquad\left.+\left(\sigma^-_{j+\frac{1}{2}}+\sigma^+_{j-\frac{1}{2}}\right)\left(h^-_{1,j+\frac{1}{2}}-h^+_{1,j-\frac{1}{2}}\right)\right].
\end{aligned}\tag{47}$$

This factorization of the numerical flux(es) difference (42) (and (43)), suggest the following balanced discretization of the source term integrals on the right hand side of (22)

$$\begin{aligned}
&\int_{x^-_{j\pm\frac{1}{2}}}^{x^+_{j\pm\frac{1}{2}}}\left(\widehat{w}_2h_1\sigma'+\sigma\widehat{w}_2\frac{\partial h_1}{\partial x}\right)dx\\
&\quad\approx\frac{\widehat{w}^+_{2,j\pm\frac{1}{2}}+\widehat{w}^-_{2,j\pm\frac{1}{2}}}{2}\cdot\frac{h^+_{1,j\pm\frac{1}{2}}+h^-_{1,j\pm\frac{1}{2}}}{2}\cdot\left(\sigma^+_{j\pm\frac{1}{2}}-\sigma^-_{j\pm\frac{1}{2}}\right)\\
&\qquad+\frac{\sigma^+_{j\pm\frac{1}{2}}+\sigma^-_{j\pm\frac{1}{2}}}{2}\cdot\frac{\widehat{w}^+_{2,j\pm\frac{1}{2}}+\widehat{w}^-_{2,j\pm\frac{1}{2}}}{2}\cdot\left(h^+_{1,j\pm\frac{1}{2}}-h^-_{1,j\pm\frac{1}{2}}\right),
\end{aligned}\tag{48}$$

for the integrals across the cell interfaces at $x_{j\pm\frac{1}{2}}$, and

$$\begin{aligned}
&\int_{x^+_{j-\frac{1}{2}}}^{x^-_{j+\frac{1}{2}}}\left(\widehat{w}_2h_1\sigma'+\sigma\widehat{w}_2\frac{\partial h_1}{\partial x}\right)dx\\
&\quad\approx\frac{\widehat{w}^-_{2,j+\frac{1}{2}}+\widehat{w}^+_{2,j-\frac{1}{2}}}{2}\cdot\frac{h^-_{1,j+\frac{1}{2}}+h^+_{1,j-\frac{1}{2}}}{2}\cdot\left(\sigma^-_{j+\frac{1}{2}}-\sigma^+_{j-\frac{1}{2}}\right)\\
&\qquad+\frac{\sigma^-_{j+\frac{1}{2}}+\sigma^+_{j-\frac{1}{2}}}{2}\cdot\frac{\widehat{w}^-_{2,j+\frac{1}{2}}+\widehat{w}^+_{2,j-\frac{1}{2}}}{2}\cdot\left(h^-_{1,j+\frac{1}{2}}-h^+_{1,j-\frac{1}{2}}\right),
\end{aligned}\tag{49}$$

for the integral of the source term across the cell I_j. And similarly,

$$\begin{aligned}
&\int_{x^-_{j\pm\frac{1}{2}}}^{x^+_{j\pm\frac{1}{2}}} \left(w_2 h_2 \sigma' + \sigma w_2 \frac{\partial h_2}{\partial x} \right) dx \\
&\quad \approx \frac{w^+_{2,j\pm\frac{1}{2}} + w^-_{2,j\pm\frac{1}{2}}}{2} \cdot \frac{h^+_{2,j\pm\frac{1}{2}} + h^-_{2,j\pm\frac{1}{2}}}{2} \cdot \left(\sigma^+_{j\pm\frac{1}{2}} - \sigma^-_{j\pm\frac{1}{2}} \right) \\
&\qquad + \frac{\sigma^+_{j\pm\frac{1}{2}} + \sigma^-_{j\pm\frac{1}{2}}}{2} \cdot \frac{w^+_{2,j\pm\frac{1}{2}} + w^-_{2,j\pm\frac{1}{2}}}{2} \cdot \left(h^+_{2,j\pm\frac{1}{2}} - h^-_{2,j\pm\frac{1}{2}} \right),
\end{aligned} \tag{50}$$

and

$$\begin{aligned}
&\int_{x^+_{j-\frac{1}{2}}}^{x^-_{j+\frac{1}{2}}} \left(w_2 h_2 \sigma' + \sigma w_2 \frac{\partial h_2}{\partial x} \right) dx \\
&\quad \approx \frac{w^-_{2,j+\frac{1}{2}} + w^+_{2,j-\frac{1}{2}}}{2} \cdot \frac{h^-_{2,j+\frac{1}{2}} + h^+_{2,j-\frac{1}{2}}}{2} \cdot \left(\sigma^-_{j+\frac{1}{2}} - \sigma^+_{j-\frac{1}{2}} \right) \\
&\qquad + \frac{\sigma^-_{j+\frac{1}{2}} + \sigma^+_{j-\frac{1}{2}}}{2} \cdot \frac{w^-_{2,j+\frac{1}{2}} + w^+_{2,j-\frac{1}{2}}}{2} \cdot \left(h^-_{2,j+\frac{1}{2}} - h^+_{2,j-\frac{1}{2}} \right),
\end{aligned} \tag{51}$$

for the integrals of the source terms corresponding to the discharge of the top layer, Q_2.

We observe that the approximations (48)–(49) balance exactly the right hand side of (42), and (50)–(51) that of (43), provided properties $\mathcal{P}_4$ and $\mathcal{P}_5$ are satisfied. With this discretization, the right hand side of the discharge equations in (22) vanishes for steady-state of rest.

To ensure preservation of total water height of the first layer, w_1, and the height of the second layer, h_2, over time, the first and third components of the numerical fluxes, $H^{\overline{A}^T_1}_{j\pm\frac{1}{2}}$ and $H^{A_2}_{j\pm\frac{1}{2}}$, must be calculated so that their differences yield

$$\frac{d\overline{A}^T_{1,j}}{dt} = 0, \quad \text{and} \quad \frac{d\overline{A}_{2,j}}{dt} = 0 \tag{52}$$

when $w_1 = \text{Const.}$, $h_2 = \text{Const.}$, and $u_i \equiv 0$ $(i = 1, 2)$. To this end, we approximate the interface jump of the total area of the first layer in the numerical flux in (22) by

$$\begin{aligned}
A^{T,+}_{1,j+\frac{1}{2}} - A^{T,-}_{1,j+\frac{1}{2}} &\equiv \sigma\left(x^+_{j+\frac{1}{2}}\right) w_1\left(x^+_{j+\frac{1}{2}}, t\right) - \sigma\left(x^-_{j+\frac{1}{2}}\right) w_1\left(x^-_{j+\frac{1}{2}}, t\right) \\
&\approx \sigma_{j+\frac{1}{2}} \left(w^+_{1,j+\frac{1}{2}} - w^-_{1,j+\frac{1}{2}} \right),
\end{aligned} \tag{53}$$

and the wet area of the second layer as

$$\begin{aligned}
A^+_{2,j+\frac{1}{2}} - A^-_{2,j+\frac{1}{2}} &\equiv \sigma\left(x^+_{j+\frac{1}{2}}\right) h_2\left(x^+_{j+\frac{1}{2}}, t\right) - \sigma\left(x^-_{j+\frac{1}{2}}\right) h_2\left(x^-_{j+\frac{1}{2}}, t\right) \\
&\approx \sigma_{j+\frac{1}{2}} \left(h^+_{2,j+\frac{1}{2}} - h^-_{2,j+\frac{1}{2}} \right),
\end{aligned} \tag{54}$$

where

$$\sigma_{j+\frac{1}{2}} = \max\left\{ \widetilde{\sigma}^-_{j+\frac{1}{2}}, \widetilde{\sigma}^+_{j+\frac{1}{2}} \right\}, \tag{55}$$

with

$$\widetilde{\sigma}^{-}_{j+\frac{1}{2}} := \frac{A^{T,-}_{1,j+\frac{1}{2}}}{w^{-}_{1,j+\frac{1}{2}}} \quad \text{and} \quad \widetilde{\sigma}^{+}_{j+\frac{1}{2}} := \frac{A^{T,+}_{1,j+\frac{1}{2}}}{w^{+}_{1,j+\frac{1}{2}}}. \tag{56}$$

Remarks

1. For smooth channel geometries, i.e., $B^{-}_{j+\frac{1}{2}} = B^{+}_{j+\frac{1}{2}}$ and $\sigma^{-}_{j+\frac{1}{2}} = \sigma^{+}_{j+\frac{1}{2}}$, both the interface jump of the flux (first and third differences on the right hand side of (44) and the corresponding terms in the equation for Q_2) and the integrals of the source term across the cell interfaces, (48) and (50), vanish for the steady-state of rest, (12). For other steady-states, even when $B(x)$ is smooth, this cancellation may not occur, as h_1 and h_2 may jump across the cell interfaces.
2. Approximating $A^{T,+}_{1,j+\frac{1}{2}} - A^{T,-}_{1,j+\frac{1}{2}}$ and $A^{+}_{2,j+\frac{1}{2}} - A^{-}_{2,j+\frac{1}{2}}$ respectively by (53) and (54) ensures that these terms vanish for steady-states of rest as required.
3. The choice of $\sigma_{j\pm\frac{1}{2}}$ in (53) ensures positive values of the cell average of the water height $\overline{h}_{1,j}(t+\Delta t)$ (see Appendix A); other choices are possible within the second order accuracy of the scheme.

2.5 Time Evolution

Given the reconstructed interface values at time t as described in Sect. 2.2,

$$v^{\pm}_{j\pm\frac{1}{2}}(t) = \begin{pmatrix} A^{T,\pm}_{1,j\pm\frac{1}{2}}(t) \\ Q^{\pm}_{1,j\pm\frac{1}{2}}(t) \\ A^{\pm}_{2,j\pm\frac{1}{2}}(t) \\ Q^{\pm}_{2,j\pm\frac{1}{2}}(t) \end{pmatrix}, \tag{57}$$

we estimate the maximum interface wave speeds of (15a)–(15d) as the maximum speed of propagation as given by the first order approximation (6a)–(6b).

$$a_{j\pm\frac{1}{2}} = \max_i \left|\lambda_i(x_{j\pm\frac{1}{2}})\right|, \tag{58}$$

and the ODE system (22) is numerically integrated using the second order *Strong Stability Preserving* Runge-Kutta scheme, [9, 25],

$$v^{(1)} = v^{(0)} + \Delta t C\big[v^{(0)}\big] \tag{59a}$$

$$v^{(2)} = \frac{1}{2}v^{(0)} + \frac{1}{2}\big(v^{(1)} + \Delta t C\big[v^{(1)}\big]\big) \tag{59b}$$

$$\overline{v}(t+\Delta t) := v^{(2)}, \tag{59c}$$

with the numerical fluxes

$$C\big[v(t)\big] = -\frac{H_{j+\frac{1}{2}}(v(t)) - H_{j-\frac{1}{2}}(v(t))}{\Delta x} + \overline{S}_j(t) \tag{60}$$

where $H_{j\pm\frac{1}{2}}$ is given by (19), using (53) and (54), and the integrals of the source terms appearing on the right of (22) approximated by (48)–(51).

2.6 Properties of the Scheme and Additional Remarks

To conclude this section, we summarize the two main properties of the semi-discrete central scheme resulting from applying the discretization of the source term (48)–(51), along with the reconstruction (32)–(38), and the SSP Runge-Kutta solver (59a), (59b), (60) to the semi-discrete central formulation (22). (We defer the proofs of the following theorems to Appendix A).

Theorem 1 *Consider the balance law* (15a)–(15d) *and the semi-discrete central formulation* (22) *with the spatial integrals of the source term approximated by* (48)–(51), *the interface pointvalues of* $w_1(x,t)$ *and* $h_1(x,t)$ *given by* (36)–(37) *and* (38), *those of* $A_1^T(x,t)$, $A_2(x,t)$, $h_2(x,t)$, *and* $Q_i(x,t)$ $(i=1,2)$ *recovered by the minmod reconstruction* (32)–(34), *with* $w_2(x,t)=w_1(x,t)+h_2(x,t)$ *and* $\widehat{w}_2(x,t)=w_1(x,t)+rh_2(x,t)$, *and the jump of the total area of the first layer and wet area of the second layer across the cell interfaces approximated by* (53)–(55). *Then*

(i) *the system of ODEs* (22) *satisfies*

$$\frac{d}{dt}\begin{pmatrix}\overline{A}^T_{1,j}(t)\\ \overline{A}_{2,j}(t)\\ \overline{Q}_{1,j}(t)\\ \overline{Q}_{2,j}(t)\end{pmatrix}=0 \quad \forall j, \tag{61}$$

for $w_1=\text{Const.}$, $h_2=\text{Const.}$, *and* $u_i\equiv 0$ $(i=1,2)$, *i.e., the central scheme is well-balanced, and*

(ii) *if the cell averages* $\overline{A}^T_1(t)$ *are such that*

$$\overline{w}_{1,j}(t)-\overline{B}_j\geq 0, \quad \forall j, \tag{62}$$

then, the cell averages $\overline{A}^T_1(t+\Delta t)$ *as evolved with forward Euler's method* (59a) *and* (60) *under the* CFL *limitation*,

$$\frac{\Delta t}{\Delta x}<\frac{\sigma_j}{2a_j} \quad \forall j, \tag{63}$$

where $a_j=\max\{a_{j-\frac{1}{2}}\sigma_{j-\frac{1}{2}}, a_{j+\frac{1}{2}}\sigma_{j+\frac{1}{2}}\}$, *will yield*

$$\overline{w}_{1,j}(t+\Delta t)-\overline{B}_j\geq 0, \quad \forall j. \tag{64}$$

3 Numerical Results

In this section we present the numerical solutions of several prototype problems aimed at demonstrating the properties of our central scheme and its ability to capture non-trivial steady flows. We begin by validating the well balance property of the scheme and its behavior under small perturbations from the trivial steady-state, (12). We also evolve two sets

of initial conditions that lead to delicate wave structures so as to validate the ability of our *Riemann solver free* scheme to correctly detect and propagate these waves along the interface of the two water layers. To conclude, we study the convergence of solutions evolved with the central scheme to non-trivial steady-state solutions by comparing them to steady flows computed under the rigid-lid assumption, $h_1 + h_2 + B = H_o$.

The flows are calculated along channels with varying width and bottom topography. For each flow we consider different cases according to the location of the narrowest point along the channel with respect to the location of the maximum elevation of the bottom topography along the solution domain.

For modeling stratified flows, the regime $r \approx 1$ is of particular interest, so unless otherwise stated, for the results presented below, we follow [1–3, 7, 8, 16, 21] and set the ratio of densities $r = \frac{\rho_2}{\rho_1} = 0.98$, the value of the acceleration of gravity is taken as $g = 9.81$, and the time step, Δt, satisfies the CFL restriction

$$\Delta t \leq \frac{\tau \Delta x}{\max_j \{a_{j+\frac{1}{2}}\}}, \quad \tau < 1, \tag{65}$$

where $a_{j+\frac{1}{2}}$ stands for an estimate of the spectral radius of the modified Jacobian (4). To this end, using the bounds provided in [1], we let

$$c_1 = \sqrt{g h_1} \quad \text{and} \quad c_2 = \sqrt{g h_2}, \tag{66}$$

and order the estimates for the external eigen values, (6b)

$$\mu_1 = \min\left\{u_1 - \sqrt{1+\sqrt{r}}c_1, u_2 - \sqrt{1+\sqrt{r}}c_2\right\} \tag{67a}$$

$$\mu_2 = \max\left\{u_1 + \sqrt{1+\sqrt{r}}c_1, u_2 + \sqrt{1+\sqrt{r}}c_2\right\}, \tag{67b}$$

to bound the maximum speed of propagation at each cell interface by

$$a_{j+\frac{1}{2}} = \max\left\{|\mu_1|, |\mu_2|\right\}. \tag{68}$$

We note here that while the proof of Theorem 1 requires $\tau < \frac{1}{2}$, except for the interface propagation problems, all the numerical experiments below were computed with values $\frac{1}{2} < \tau < 1$. The same flows simulated with a more restrictive CFL number, $\tau < \frac{1}{2}$, did not yield substantially better results.

3.1 Steady-State of Rest and Small Perturbation from Rest

We begin by testing the well balance property of the scheme, Theorem 1, for the steady-state of rest and small deviations from it.

3.1.1 The Trivial Steady-State of Rest

In order to test the well balance property, we evolve the conditions describing the steady-state of rest,

$$u_1(x,0) = u_2(x,0) = 0, \qquad w_1(x,0) = -1, \quad \text{and} \quad h_2(x,0) = 1. \tag{69}$$

These initial conditions are evolved over a smooth bottom topography given by

$$B(x) = \begin{cases} \frac{1}{4}(1 + \cos\frac{\pi(x-0.5)}{0.1}) - 2 & \text{if } 0.4 \le x \le 0.6, \\ -2 & \text{otherwise,} \end{cases} \tag{70}$$

and also over a discontinuous bottom given by the step function

$$B(x) = \begin{cases} -2 & \text{if } x \le 0.5, \\ -1.7 & \text{if } x > 0.5, \end{cases} \tag{71}$$

Solutions computed up to $t = 5$ using 200 grid cells and different channel configurations with parabolic contractions of up to 50 % at the narrowest section of the channel confirm the well balance property of the scheme. In all cases the total height of the layers, w_i $(i = 1, 2)$ remains constant, and the deviations from rest of the flow velocities, u_i $(i = 1, 2)$, are in the order of 10^{-16}, clearly produced by the round-off error in the computer's arithmetic operations.

3.1.2 Perturbation from Rest

Next, we test the behavior of the scheme when a small perturbation is added to the initial profile of h_2 in (69),

$$h_2(x, 0) = \begin{cases} 1 + 10^{-5} & \text{if } 0.1 < x < 0.2, \\ 1 & \text{otherwise.} \end{cases} \tag{72}$$

Figure 3 shows the initial conditions and several snapshots of the evolution of the perturbation up to $t = 0.26$. Convergence to the trivial equilibrium solution, (69), is observed for both bottom topographies, (70) and (71) and contractions of up to 50 %.

3.2 Interface Propagation

The following two examples are aimed at validating the ability of our scheme to capture and propagate discontinuities over time. In both cases an initial jump on the height of the interface between the two fluid layers, $w_1 = h_1 + B$, leads to a time dependent solution consisting of four traveling waves. These examples have been widely used to validate schemes for multilayer flows, [1, 7, 15]. The initial conditions for the first one are given by

$$(h_1, Q_1, h_2, Q_2) = \begin{cases} (0.5, 1.25, 0.5, 1.25) & \text{if } x < 0, \\ (0.55, 1.375, 0.45, 1.125) & \text{if } x > 0. \end{cases} \tag{73}$$

The channel is straight, $\sigma(x) = 1$, with a flat bottom placed at $B(x) = -1$ and extending over the interval $x \in [0, 1]$. We approximate the solution over three different grids of sizes $\Delta x = 1/400, 1/800, 1/10,000$ and observe how the increased resolution allows us to capture the sharp profile that characterizes the solution and reduces the amplitude of oscillations. Figure 4 shows the elevation of the interface between the two layers, the velocity of each layer, and the small displacement of the free surface of the flow caused by the propagating discontinuities.

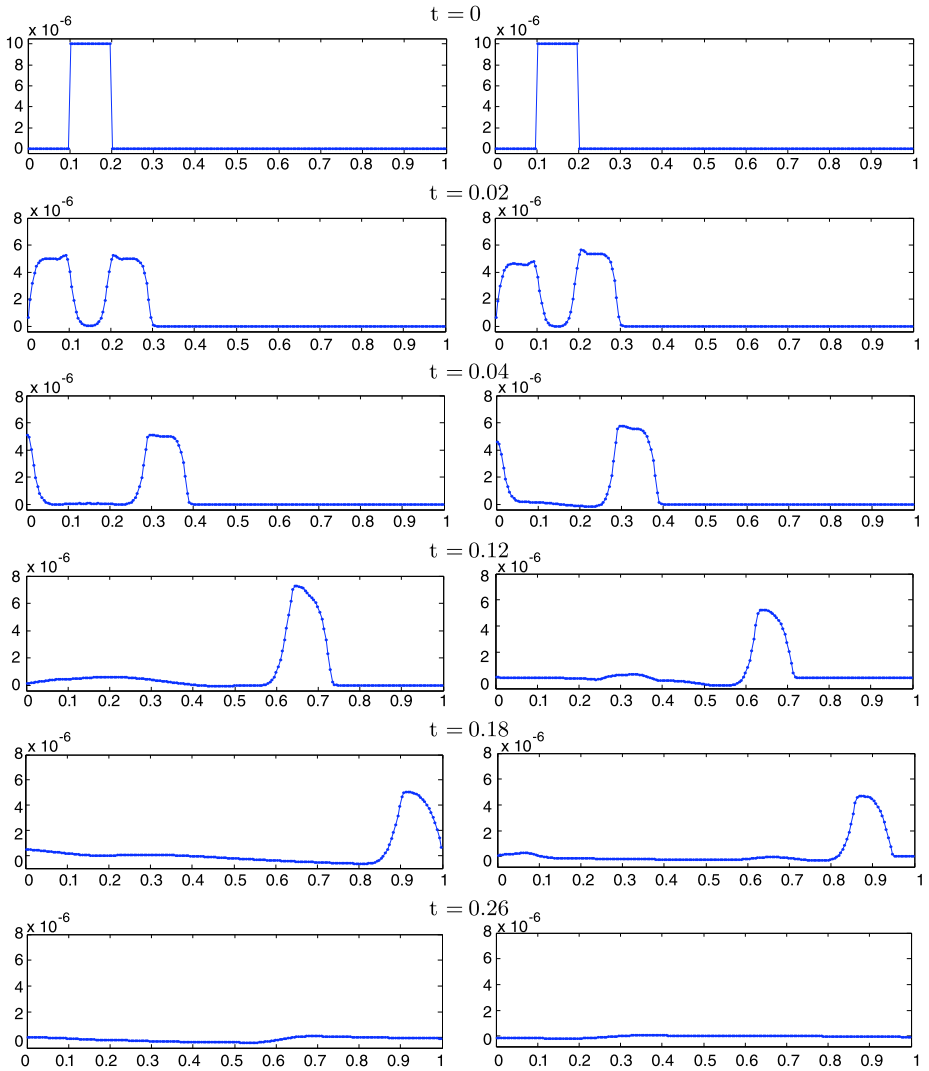

Fig. 3 Evolution of the total height of the perturbed state of rest, (72), along channels with different configurations. *Left*: flow through a channel with a parabolic contraction with its narrowest point (50 %) located to the right of the maximum elevation of the bottom topography given by (70). *Right*: parabolic contraction of 40 % located to the left of a step in the bottom of the channel, (71). Solutions computed with 200 grid cells and CFL number 0.75

In the second example, we also consider a straight channel with a flat bottom, and the initial conditions are given by the piecewise data

$$(h_1, Q_1, h_2, Q_2) = \begin{cases} (0.2, 0, 1.8, 0) & \text{if } x < 0 \\ (1.8, 0, 0.2, 0) & \text{if } x > 0 \end{cases} \tag{74}$$

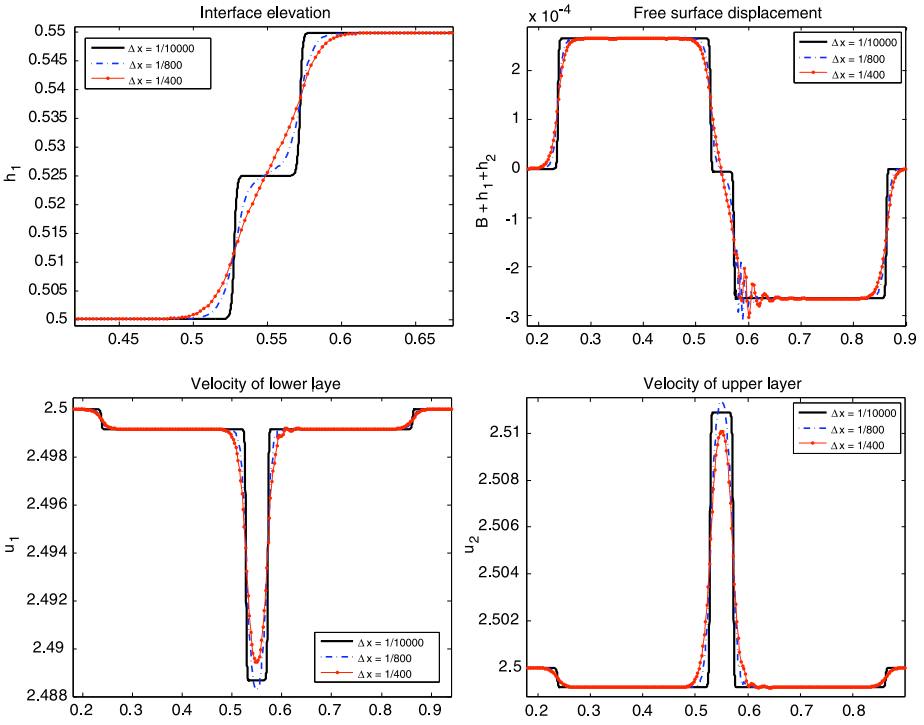

Fig. 4 First interface propagation problem. *Top*: *left*: interface elevation, *right*: free surface displacement. *Bottom*: *left*: velocity of lower layer, *right*: velocity of upper layer. Solutions computed with CFL number 0.5

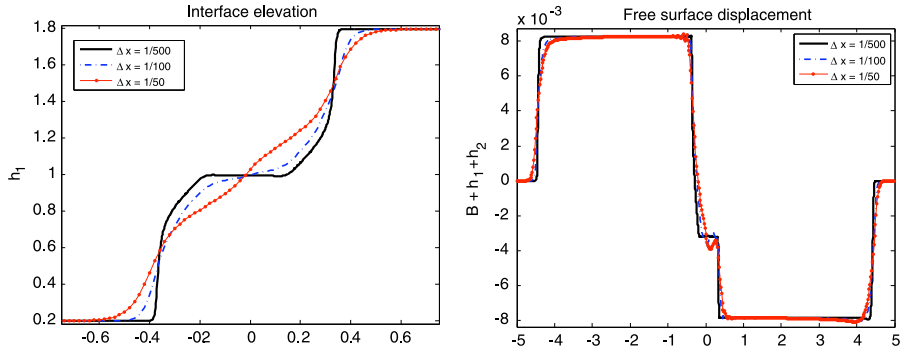

Fig. 5 First interface propagation problem. *Left*: interface elevation, *right*: free surface displacement. Solutions computed with CFL number 0.75

In this case we compute the solution from $x = -5$ to $x = 5$ using grid sizes $\Delta x = 1/500, 1/100, 1/50$. The results displayed in Fig. 5 confirm the ability of the proposed scheme to locate and resolve the discontinuities in the solution.

3.3 Non-trivial Steady-States

In this section we investigate the ability of our scheme to capture accurately non-trivial steady flows given by (11a)–(11c). Steady and quasi-steady flows occur commonly in nature

(e.g., channel and river flows with constant discharge, strait flows between large steady basins). Such flows are well modeled by system (1a)–(1d) and under the—reasonable—*rigid lid* assumption, $B + h_1 + h_2 = \text{Const.}$—its actual displacement is of order $\mathcal{O}(1 - r)$, one can calculate exact solutions for them, [1–3, 7, 8, 21, 27, 28]. These flows are fully determined by the conditions at the *inflow* and *outflow* boundaries and the geometry of the channel. That is, given $B(x)$, $\sigma(x)$, and the values Q_1, Q_2, h_1^{out}, and h_2^{out}, in addition to the rigid lid value $H_o = h_1 + h_2 + B$, one can determined the flow conditions at each point along the solution domain. The analysis of these flows is presented in great detail in [2, 3, 8], and algorithms to calculate their rigid lid solutions are provided in [1, 21, 28]. We consider flows in three distinct regimes given by the value of the composite Froude number, G^2, (14): subcritical or fluvial flows, for which $G^2 < 1$ along the entire channel, and two types of transcritical flows, for which G^2 changes from subcritical, $G^2 < 1$, to supercritical, $G^2 > 1$, along the channel due to the varying geometry. Once a transcritical flow reaches criticality, it may remain supercritical through the outflow boundary, or it may *jump* back to subcritical conditions by dissipating energy through a *shock* (see Sect. 3.3.3). Below, we consider all these different flow regimes along channels with varying geometries, and compare the approximate solutions computed with our scheme with the generalized rigid lid solutions.

3.3.1 Subcritical Flow

We first consider a subcritical flow along a straight channel extending over the interval $x \in [-3, 3]$ with

$$Q_1 = -Q_2 = -0.05, \qquad h_1^{\text{out}}(x) = -1.5 - B(x), \quad \text{and} \quad h_2^{\text{out}} = 0.5, \tag{75}$$

and the bottom topography given by

$$B(x) = 0.85e^{-x^2} - 2. \tag{76}$$

We then add a contraction of the form

$$\sigma(x) = 1 - be^{-c(x-a)^2}, \tag{77}$$

for different values of a, b and c, while keeping the flow invariants, Q_1, Q_2, h_1^{out}, and h_2^{out}, unchanged, and observe the effect that the narrowing contraction and its change in location (with respect to the highest bottom elevation) have in the flow. In all cases, the initial conditions are set to the prescribed boundary values throughout the entire domain. The results are presented in Figs. 6, 7 and 8.

3.3.2 Lock Exchange Flows

Next, we consider two exchange flows proposed in [7]. In the first problem the two layers of water are initially at rest separated by a membrane. When the membrane is removed and the two masses are allowed to flow, they do so in opposite directions. In the second example, a less dense mass of water lays on top of a heavier one and both layers are initially separated from two reservoirs at each end of the channel, when the membranes are removed at $t = 0$, the two layers flow until they match the conditions of the corresponding layers at each reservoir. These are known as lock exchange flows and they converge to steady-states whose exact rigid lid solution, [2], can be computed with arbitrary accuracy, [21]. Lock

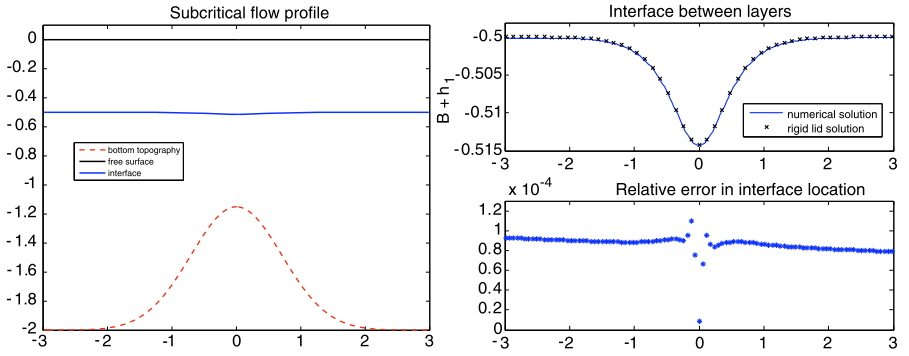

Fig. 6 *Left*: profile of a subcritical flow along a straight channel. *Right*: detail of interface elevation (*top*), and its relative error (*bottom*). Solutions calculated with 200 grid cells and CFL number 0.75

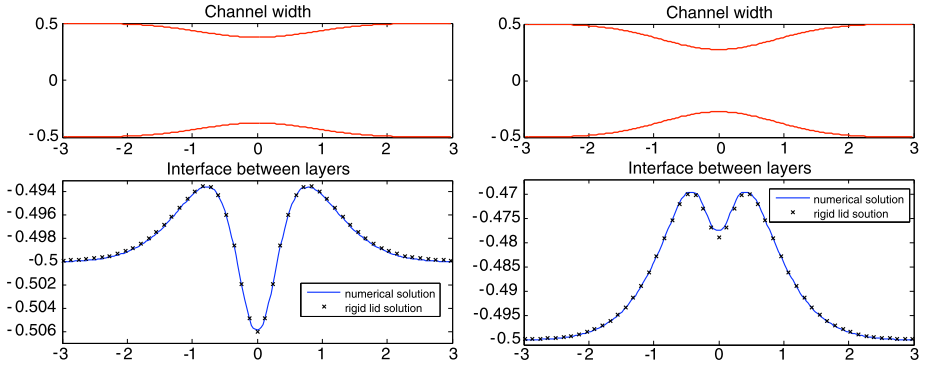

Fig. 7 Interface location for two subcritical flows running through the corresponding centered contractions depicted above. *Left*: 25 % contraction. *Right*: 45 % contraction. Solutions calculated with 200 grid cells and CFL number 0.75

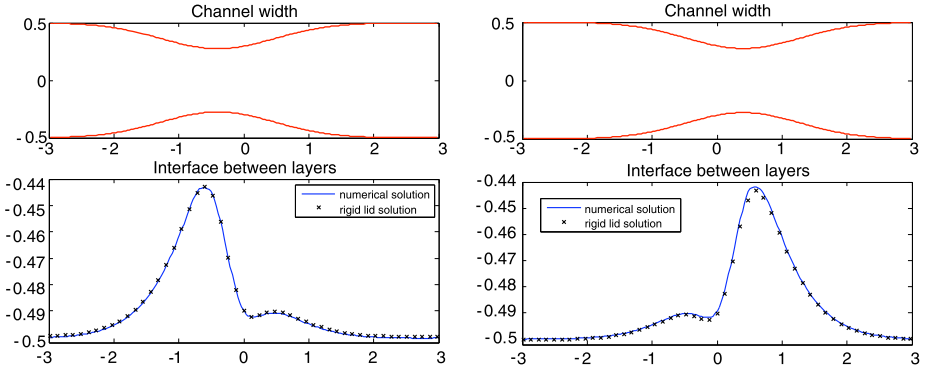

Fig. 8 Interface location for two subcritical flows running through the corresponding shifted contractions depicted above. *Left*: 45 % contraction with narrowest point located at $x = -0.4$. *Right*: 45 % contraction with narrowest point located at $x = 0.4$. Solutions calculated with 200 grid cells and CFL number 0.75

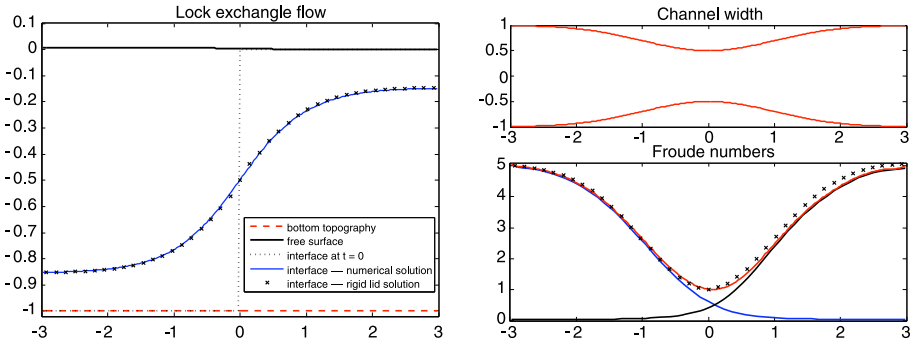

Fig. 9 Lock exchange flow. *Left*: Flow profile. *Right*: *top*: channel width, *bottom*: Froude numbers F_1^2 and F_2^2 (*solid lines*), G^2 (∘'s) from numerical solution, and G^2 from rigid lid solution (×'s). Solutions calculated with 200 grid cells and CFL number 0.75

exchange flows are characterized by the loss of strict hyperbolicity, [7], posing an additional difficulty for calculating their numerical solutions, especially for schemes that require a Riemann solver for their implementation. Our semi-discrete central scheme is particularly well suited for simulating these flows as it only requires a bound such as (68) for the largest external eigen value (which is always real) for its implementation.

In the first case, we simulate a maximal exchange flow (i.e., the exchange of momentum between the layers is maximum for the given channel geometry) through a channel with constant depth, $B(x) = -1$, and a contraction given by

$$\sigma(x) = 2 - e^{-x^2/2}. \tag{78}$$

The initial conditions are given by

$$(h_1, Q_1, h_2, Q_2) = \begin{cases} (1, 0, 0, 0) & \text{if } x < 0, \\ (0, 0, 1, 0) & \text{if } x > 0, \end{cases} \tag{79}$$

and at each boundary we impose the condition $Q_1 = -Q_2$. Figure 9 displays the numerical and rigid solutions for this flow along with the Froude numbers of the flow.

In the second lock exchange experiment we consider a flow through a channel extending from $x = -1$ to $x = 2$ consisting of a combination of a sill described by

$$B(x) = \frac{1}{\cosh^2(3.75x)} - 2, \tag{80}$$

and a contraction given by

$$\sigma(x) = 0.5 + 1.5\left(1 - e^{-a^2(x-1)^2}\right), \quad \text{with } a = \begin{cases} 0.637 & \text{if } x \le 1, \\ 1.273 & \text{if } x > 1. \end{cases} \tag{81}$$

The initial conditions are set to

$$h_1 = 1.3, \qquad h_2 = 0.7, \qquad Q_1 = Q_2 = 0. \tag{82}$$

At the left boundary, where the flow is supercritical, we set the discharge of the top layer, Q_2, to the value given by the rigid lid solver, and at the right end, where the flow is subcritical,

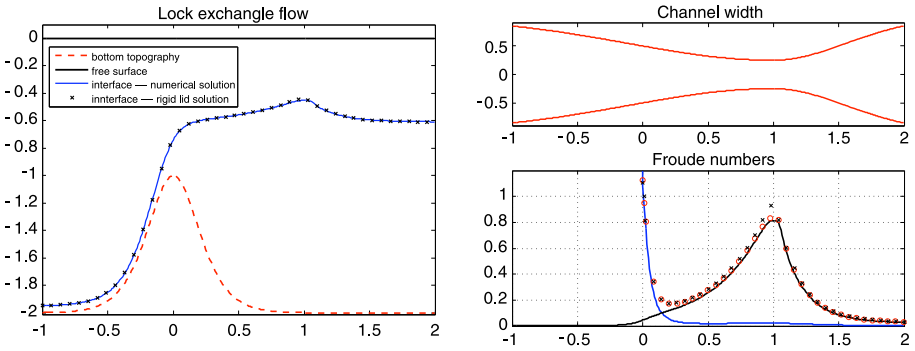

Fig. 10 Lock exchange flow through a combination of a sill and a contraction. *Left*: Flow profile. *Right*: *top*: channel width, *bottom*: Froude numbers F_1^2 and F_2^2 (*solid lines*), G^2 ($\circ$'s) from numerical solution, and G^2 from rigid lid solution ($\times$'s). Solution calculated with 300 grid cells and CFL number 0.75

we specify both discharges, and the elevation of each layer so as to match the conditions at the reservoir as given by the rigid lid solver. The numerical solution is presented in Fig. 10 along with the rigid lid solution and the internal and composite Froude numbers for the flow.

3.3.3 Internal Dam Break

In this last experiment an internal dam break is simulated. The two layers, initially at rest separated by a membrane, are left to flow through a channel extending over the interval $x \in [-5, 5]$ with bottom topography

$$B(x) = 1.2e^{-2(x+1)^2} - 2, \tag{83}$$

and a contraction described by

$$\sigma(x) = 1 - 0.4e^{-(x-1)^2/8}. \tag{84}$$

And the initial conditions are set to

$$(h_1, Q_1, h_2, Q_2) = \begin{cases} (\max(0, -1.5 - B(x)), 0, 2 - h_1 + B(x), 0) & \text{if } x < -1, \\ (1.5, 0, 0.5, 0) & \text{if } x > -1, \end{cases} \tag{85}$$

At the boundaries, we specify the values of h_1, h_2, Q_1, and Q_2 given by the rigid lid solution. In this case the flow is subcritical at the right boundary, accelerates through the contraction, with the upper layer nearly reaching criticality at that point, remaining subcritical until it flows over the top of the sill, and then connects to the subcritical conditions at the left end by dissipating energy through a stationary shock. The flow presented in Fig. 11 demonstrate the ability of the proposed central scheme to locate and resolve the stationary jump in the interface.

4 Conclusions

The numerical results presented in Sect. 3 demonstrate the robustness and versatility of the proposed central schemes for computing the numerical solution of one-dimensional two-layer shallow-water flows along channels with rectangular cross-section. The balance law

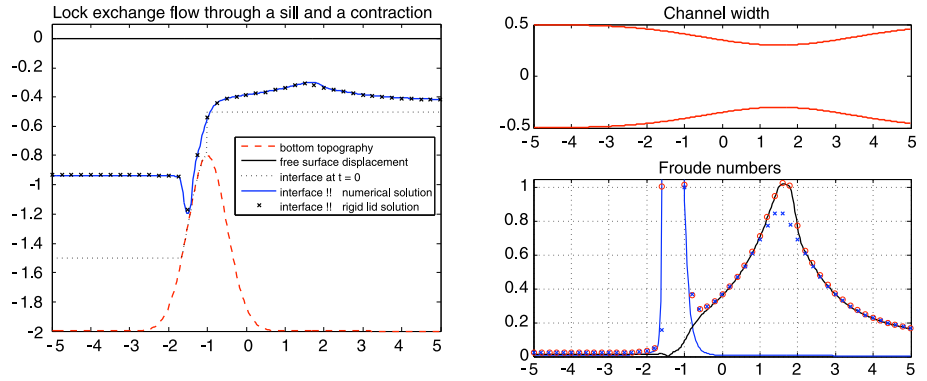

Fig. 11 Internal dam break flow. *Left*: Flow profile. *Right*: *top*: channel width, *bottom*: Froude numbers F_1^2 and F_2^2 (*solid lines*), G^2 (∘'s) from numerical solution, and G^2 from rigid lid solution (×'s). Solution calculated with 300 grid cells and CFL number 0.75

(1a)–(1d) that models these flows includes non-conservative products that make the balancing of fluxes and sources more challenging than in one-layer flows, and renders a more characteristic decomposition of the system, including the possible loss of hyperbolicity for steady-state flows. Our results demonstrate that central schemes can handle these difficulties robustly, and that they are particularly well suited to deal with the loss of hyperboliciy as they only require an estimate of the maximum speed of propagation.

Acknowledgements This work was partially supported by NSF award DMS # 0609766

Appendix A: Proof of Theorem 1

Proof (i) Starting with the initial conditions $u_i(x) = 0$ $(i = 1, 2)$, $w_1(x) = W_1$ and $h_2(x) = H_2$ for all x, we fix a space scale Δx and the corresponding partition of the solution domain, $\{I_j\} := \{[x_{j-\frac{1}{2}}, x_{j+\frac{1}{2}}]\}$. We then define the cell averages of the conserved quantities in the modified shallow-water model, (15a)–(15d), as

$$\overline{A}^T_{1,j} := \overline{\sigma}_j \overline{w}_{1,j} = \overline{\sigma}_j W_1 \quad \text{and} \quad A_{2,j} := \overline{\sigma}_j \overline{h}_{2,j} = \overline{\sigma}_j H_2 \tag{86}$$

and

$$\overline{Q}_{1,j} := \big(\overline{A}^T_{1,j} - \overline{\sigma}_j \overline{B}_j\big)\overline{u}_{1,j} \equiv 0. \tag{87a}$$

$$\overline{Q}_{2,j} := A_{2,j}\overline{u}_{2,j} \equiv 0. \tag{87b}$$

The reconstructed point values of w_1 and h_2, clearly satisfy $w^{\pm}_{1,j\pm\frac{1}{2}} = W_1$, $h_{2,j\pm\frac{1}{2}} = H_2$, and those of Q_i, $Q^{\pm}_{j\pm\frac{1}{2}} = 0$ $(i = 1, 2)$, thus the values of the water heights (38) (and the corresponding values of h_2 recovered via the minmod reconstruction), and those of the bottom topography at the cell interfaces, $B^{\mp}_{j\pm\frac{1}{2}}$, satisfy

$$h^-_{1,j+\frac{1}{2}} - h^+_{1,j-\frac{1}{2}} = -\big(B^-_{j+\frac{1}{2}} - B^+_{j-\frac{1}{2}}\big) \quad \text{and} \quad h^-_{2,j+\frac{1}{2}} - h^+_{2,j-\frac{1}{2}} = 0 \tag{88}$$

In view of this, the first and third components of the numerical fluxes $H_{j+\frac{1}{2}}$ in (22) read

$$-\frac{H^{(1)}_{j+\frac{1}{2}}-H^{(1)}_{j-\frac{1}{2}}}{\Delta x}=-\frac{1}{2\Delta x}\big[a_{j+\frac{1}{2}}\sigma_{j+\frac{1}{2}}\big(w^{+}_{1,j+\frac{1}{2}}-w^{-}_{1,j+\frac{1}{2}}\big)-a_{j-\frac{1}{2}}\sigma_{j-\frac{1}{2}}\big(w^{+}_{1,j-\frac{1}{2}}-w^{-}_{1,j-\frac{1}{2}}\big)\big]$$
$$\equiv 0 \tag{89a}$$

$$-\frac{H^{(3)}_{j+\frac{1}{2}}-H^{(3)}_{j-\frac{1}{2}}}{\Delta x}=-\frac{1}{2\Delta x}\big[a_{j+\frac{1}{2}}\sigma_{j+\frac{1}{2}}\big(h^{+}_{2,j+\frac{1}{2}}-h^{-}_{2,j+\frac{1}{2}}\big)-a_{j-\frac{1}{2}}\sigma_{j-\frac{1}{2}}\big(h^{+}_{2,j-\frac{1}{2}}-h^{-}_{2,j-\frac{1}{2}}\big)\big]$$
$$\equiv 0. \tag{89b}$$

That is,

$$\frac{d}{dt}\overline{A}^{T}_{1,j}(t)=0 \quad\Rightarrow\quad \overline{A}^{T}_{1,j}(t+\Delta t)=\overline{A}^{T}_{1,j}(t), \tag{90a}$$

$$\frac{d}{dt}A_{2,j}(t)=0 \quad\Rightarrow\quad A_{2,j}(t+\Delta t)=A_{2,j}(t), \tag{90b}$$

which allows us to recover $\overline{w}_{1,j}(t+\Delta t)=W_1$ and $h_{2,j}(t+\Delta t)=H_2$ exactly from (86).

Noting that, according to (38), $h^{+}_{1,j+\frac{1}{2}}=h^{-}_{1,j+\frac{1}{2}}=:h_{1,j+\frac{1}{2}}$ and that the minmod reconstruction guarantees $h^{+}_{2,j+\frac{1}{2}}=h^{-}_{2,j+\frac{1}{2}}=:h_{2,j+\frac{1}{2}}$, the second and fourth components of the numerical flux amount, respectively, to (40) and (41), and since (88) hold, they are balanced by (48)–(51), therefore

$$\frac{d}{dt}\overline{Q}_{i,j}(t)=0 \quad\Rightarrow\quad \overline{Q}_{i,j}(t+\Delta t)=\overline{Q}_{i,j}(t)=0, \quad i=1,2. \tag{91}$$

and $u_{i,j}(t+\Delta t)\equiv 0$ $(i=1,2)$ are also recovered exactly.

(ii) We begin by writing explicitly the cell average $A^{T}_{1,j}(t+\Delta t)$ when the system (22) is evolved with *forward Euler's* ODE solver,

$$\overline{A}^{T}_{1,j}(t+\Delta t)=\overline{A}^{T}_{1,j}(t)-\lambda\big[H^{(1)}_{j+\frac{1}{2}}(t)-H^{(1)}_{j-\frac{1}{2}}(t)\big], \tag{92}$$

where $\lambda=\Delta t/\Delta x$. This amounts to

$$\overline{A}^{T}_{1,j}(t+\Delta t)=\overline{A}^{T}_{1,j}(t)-\frac{\lambda}{2}\big[\big(Q^{+}_{1,j+\frac{1}{2}}+Q^{-}_{1,j+\frac{1}{2}}\big)-a_{j+\frac{1}{2}}\big(A^{T,+}_{1,j+\frac{1}{2}}-A^{T,-}_{1,j+\frac{1}{2}}\big)$$
$$-\big(Q^{+}_{1,j-\frac{1}{2}}+Q^{-}_{1,j-\frac{1}{2}}\big)+a_{j-\frac{1}{2}}\big(A^{T,+}_{1,j-\frac{1}{2}}-A^{T,-}_{1,j+\frac{1}{2}}\big)\big], \tag{93}$$

(where all the terms on the right hand side are understood to be evaluated at time t). Using $Q^{\pm}_{1,j\pm\frac{1}{2}}=\sigma^{\pm}_{j\pm\frac{1}{2}}h^{\pm}_{1,j\pm\frac{1}{2}}u^{\pm}_{1,j\pm\frac{1}{2}}$, we write

$$\overline{A}^{T}_{1,j}(t+\Delta t)=\overline{A}^{T}_{1}(t)+\frac{\lambda}{2}\big[\big(a_{j+\frac{1}{2}}\sigma_{j+\frac{1}{2}}-u^{+}_{1,j+\frac{1}{2}}\sigma^{+}_{j+\frac{1}{2}}\big)h^{+}_{1,j+\frac{1}{2}}$$
$$+\big(a_{j-\frac{1}{2}}\sigma_{j-\frac{1}{2}}+u^{-}_{1,j-\frac{1}{2}}\sigma^{-}_{j-\frac{1}{2}}\big)h^{-}_{1,j-\frac{1}{2}}+a_{j+\frac{1}{2}}\sigma_{j+\frac{1}{2}}B^{+}_{j+\frac{1}{2}}+a_{j-\frac{1}{2}}\sigma_{j-\frac{1}{2}}B^{-}_{j-\frac{1}{2}}\big]$$

$$-\frac{\lambda}{2}\Big[\big(a_{j+\frac{1}{2}}\sigma_{j+\frac{1}{2}}+u^{-}_{1,j+\frac{1}{2}}\sigma^{-}_{j+\frac{1}{2}}\big)h^{-}_{1,j+\frac{1}{2}}+\big(a_{j-\frac{1}{2}}\sigma_{j-\frac{1}{2}}-u^{+}_{1,j-\frac{1}{2}}\sigma^{+}_{j-\frac{1}{2}}\big)h^{+}_{1,j-\frac{1}{2}}$$

$$+a_{j+\frac{1}{2}}\sigma_{j+\frac{1}{2}}B^{-}_{j+\frac{1}{2}}+a_{j-\frac{1}{2}}\sigma_{j-\frac{1}{2}}B^{+}_{j-\frac{1}{2}}\Big]. \tag{94}$$

The terms involving $\sigma_{j\pm\frac{1}{2}}B^{\pm}_{j\pm\frac{1}{2}}$ and $\sigma_{j\pm\frac{1}{2}}B^{\mp}_{j\pm\frac{1}{2}}$ on the right hand side cancel, and since $a_{j\pm\frac{1}{2}}\sigma_{j\pm\frac{1}{2}}\geq|u^{\pm}_{1,j\pm\frac{1}{2}}|\sigma^{\pm}_{j\pm\frac{1}{2}}$, (58), and $h^{\mp}_{1,j\pm\frac{1}{2}}\geq 0$, the CFL restriction (63) allows us to write

$$\overline{A}^{T}_{1,j}(t+\Delta t)\geq\overline{A}^{T}_{1,j}(t)-\frac{1}{2}\overline{\sigma}_{j}\big(h^{-}_{1,j+\frac{1}{2}}+h^{+}_{1,j-\frac{1}{2}}\big)=\overline{\sigma}_{j}\overline{B}_{j}, \tag{95}$$

from where (64) follows. □

Appendix B: On the Semi-Discrete Central Formulation for Hyperbolic Systems with Source Terms

The numerical scheme that we have presented in this work is based on the high-order semi-discrete central formulation for hyperbolic conservation laws first introduced in [17]. Here we outline the derivation of the equivalent semi-discrete formulation for hyperbolic systems with source terms,

$$v_t+f(v)_x=S(v,x) \tag{96}$$

Before we proceed, we should clarify that this derivation consists of three steps: staggered evolution of cell averages, reprojection onto the original non-staggered grid, and the evaluation of the limit as $\Delta t\to 0$ of the finite difference $(\overline{v}^{n+1}_{j}-\overline{v}^{n}_{j})/\Delta t$. A process that requires the formulation of several intermediate solutions presented below, however, for the actual implementation of the semi-discrete scheme one doesn't need to calculate these solutions; the intermediate solutions are only introduced formally so as to form the finite difference and take the limit.

Starting with the cell averages $\{\overline{v}^{n}_{j}\}_{j}$ over the partition $\{I_j\}_j=\{[x_{j-\frac{1}{2}},x_{j+\frac{1}{2}}]\}_j$ at time $t=t^n$, we use the estimates of the maximum speed of propagation, $a^{n}_{j+\frac{1}{2}}$, to define

$$x^{n}_{j\pm\frac{1}{2},l}:=x_{j\pm\frac{1}{2}}-a^{n}_{j\pm\frac{1}{2}}\Delta t\quad\text{and}\quad x^{n}_{j\pm\frac{1}{2},r}:=x_{j\pm\frac{1}{2}}+a^{n}_{j\pm\frac{1}{2}}\Delta t, \tag{97}$$

and with these values we repartition the computational domain into two sets of cells: the first set,

$$\{\tilde{I}_{j\pm\frac{1}{2}}\}_j=\Big\{\big[x^{n}_{j\pm\frac{1}{2},l},x^{n}_{j\pm\frac{1}{2},r}\big]\Big\}_j,$$

contains the neighborhood of the interfaces $x_{j\pm\frac{1}{2}}$ within which discontinuous solutions propagate, the second set,

$$\{\tilde{I}_{j}\}_j=\Big\{\big[x^{n}_{j-\frac{1}{2},r},x^{n}_{j+\frac{1}{2},l}\big]\Big\}_j,$$

contains the portion of the original cells where the solution remains smooth over the interval $[t^n,t^{n+1}]$ (consult Fig. 12). We then formulate two sets of *staggered* cell averages following the recipe in [11] (a non-staggered extension of the original NT scheme proposed in [22])

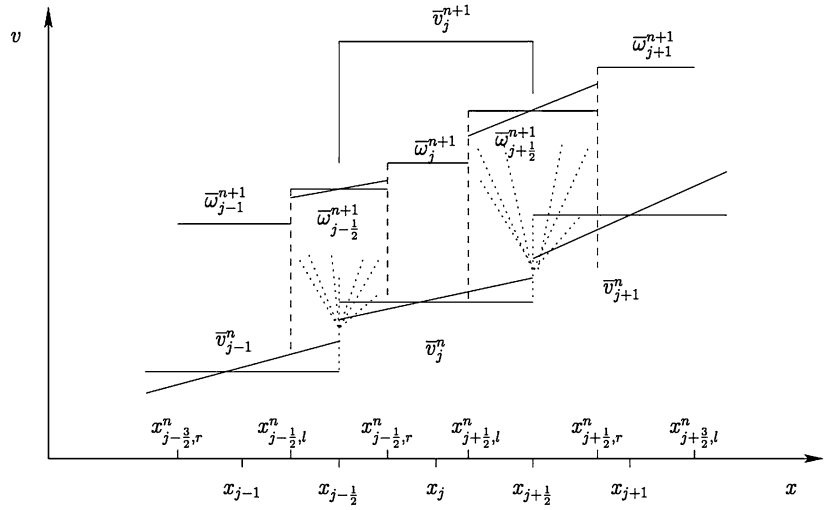

Fig. 12 Modified staggered central differencing and evolution

including, in our case, the contribution from the source term. These two sets of solutions read:

$$\overline{\omega}_{j+\frac{1}{2}}^{n+1} = \frac{\overline{v}_{j+1}^{n} + \overline{v}_j^{n}}{2} + \frac{\Delta x - a_{j+\frac{1}{2}}^{n}\Delta t}{4}\left((v_x)_{j+1}^{n} - (v_x)_j^{n}\right) - \frac{\lambda}{2a_{j+\frac{1}{2}}^{n}}\left[f\left(v_{j+\frac{1}{2},r}^{n+\frac{1}{2}}\right) - f\left(v_{j+\frac{1}{2},l}^{n+\frac{1}{2}}\right)\right]$$

$$+ \frac{\lambda}{2a_{j+\frac{1}{2}}^{n}}\int_{x_{j+\frac{1}{2},l}^{n}}^{x_{j+\frac{1}{2},r}^{n}} S\left(v^{n+\frac{1}{2}}(x), x\right)dx, \tag{98}$$

$$\overline{\omega}_j^{n+1} = \overline{v}_j^{n} + \frac{\Delta t}{2}(v_x)_j^{n} - \frac{\lambda}{1 - \lambda(a_{j-\frac{1}{2}}^{n} + a_{j+\frac{1}{2}}^{n})}\left[f\left(v_{j+\frac{1}{2},l}^{n+\frac{1}{2}}\right) - f\left(v_{j-\frac{1}{2},r}^{n+\frac{1}{2}}\right)\right]$$

$$+ \frac{\Delta t}{\Delta x - (a_{j-\frac{1}{2}}^{n} + a_{j+\frac{1}{2}}^{n})\Delta t}\int_{x_{j-\frac{1}{2},r}^{n}}^{x_{j+\frac{1}{2},l}^{n}} S\left(v^{n+\frac{1}{2}}(x), x\right)dx, \tag{99}$$

where $\lambda = \frac{\Delta t}{\Delta x}$. The midpoint values $v^{n+\frac{1}{2}}(x)$ are approximated using Taylor's theorem and the balance law (96),

$$v^{n+\frac{1}{2}}(x) \approx v^{n}(x) + \frac{\Delta t}{2}v_t^{n}(x) \approx v^{n}(x) - \frac{\Delta t}{2}\left[f\left(v^{n}(x)\right)_x - S\left(v^{n}(x), x\right)\right], \tag{100}$$

the numerical derivatives $(u_x)_j^n$ via a minmod limiter,

$$(v_x)_j^{n} = \frac{1}{\Delta x}\text{minmod}\left(\overline{v}_{j+1}^{n} - \overline{v}_j^{n}, \overline{v}_j^{n} - \overline{v}_{j-1}^{n}\right), \tag{101}$$

and the flux derivatives can be calculated as $f(v^n(x))_x = A(v)v_x$, where $A(v) = \frac{df}{dv}$ is the Jacobian matrix of f, or component by component as

$$f\big(v^n(x)\big)_x = \frac{1}{\Delta x}\text{minmod}\big(f\big(v^n(x+\Delta x)\big) - f\big(v^n(x)\big),\, f\big(v^n(x)\big) - f\big(v^n(x-\Delta x)\big)\big). \tag{102}$$

A well-balance discretization of the integrals on the right hand side of (98) can be found in [24].

From these staggered averages, we form the interpolant

$$R\big(x,t^{n+1}\big) = \sum_j \Big\{\big[\overline{\omega}^{n+1}_{j+\frac{1}{2}} + (v_x)^{n+1}_{j+\frac{1}{2}}(x - x_{j+\frac{1}{2}})\big]\mathbf{1}_{\left[x^n_{j+\frac{1}{2},l}, x^n_{j+\frac{1}{2},r}\right]} + \overline{\omega}^{n+1}_j \mathbf{1}_{\left[x^n_{j-\frac{1}{2},r}, x^n_{j+\frac{1}{2},l}\right]}\Big\} \tag{103}$$

where the derivatives $(v_x)^{n+1}_{j\pm\frac{1}{2}}$ are also approximated with a minmod limiter

$$(v_x)^{n+1}_{j+\frac{1}{2}} = \frac{2}{\Delta x}\text{minmod}\left(\frac{\overline{\omega}^{n+1}_{j+1} - \overline{\omega}^{n+1}_{j+\frac{1}{2}}}{1+\lambda(a^n_{j+\frac{1}{2}} - a^n_{j+\frac{3}{2}})}, \frac{\overline{\omega}^{n+1}_{j+\frac{1}{2}} - \overline{\omega}^{n+1}_{j}}{1+\lambda(a^n_{j-\frac{1}{2}} - a^n_{j+\frac{1}{2}})}\right). \tag{104}$$

This interpolant is then reprojected onto the original (non-staggered) grid, obtaining the updated, non-staggered cell averages

$$\begin{aligned}\overline{v}^{n+1}_j = \frac{1}{\Delta x}\int_{x_{j-\frac{1}{2}}}^{x_{j+\frac{1}{2}}} R\big(x,t^{n+1}\big)dx &= \lambda a^n_{j-\frac{1}{2}}\overline{\omega}^{n+1}_{j-\frac{1}{2}} + \big[1-\lambda\big(a^n_{j-\frac{1}{2}} + a^n_{j+\frac{1}{2}}\big)\big]\overline{\omega}^{n+1}_j \\ &+ \lambda a^n_{j+\frac{1}{2}}\overline{\omega}^{n+1}_{j+\frac{1}{2}} + \frac{\Delta x}{2}\big[\big(\lambda a^n_{j-\frac{1}{2}}\big)^2(v_x)^{n+1}_{j-\frac{1}{2}} - \big(\lambda a^n_{j+\frac{1}{2}}\big)^2(v_x)^{n+1}_{j+\frac{1}{2}}\big].\end{aligned} \tag{105}$$

In order to arrive at the semi-discrete formulation from (105), we consider the limit

$$\frac{d}{dt}\overline{v}_j(t) = \lim_{\Delta t\to 0}\frac{\overline{v}^{n+1}_j - \overline{v}^n_j}{\Delta t}. \tag{106}$$

To evaluate it, we write explicitly the finite difference using (105),

$$\begin{aligned}\frac{\overline{v}^{n+1}_j - \overline{v}^n_j}{\Delta t} &= \frac{a^n_{j-\frac{1}{2}}}{\Delta x}\overline{\omega}^{n+1}_{j-\frac{1}{2}} + \left(\frac{1}{\Delta t} - \frac{a^n_{j-\frac{1}{2}} + a^n_{j+\frac{1}{2}}}{\Delta x}\right)\overline{\omega}^{n+1}_j \\ &+ \frac{a^n_{j+\frac{1}{2}}}{\Delta x}\overline{\omega}^{n+1}_{j+\frac{1}{2}} - \frac{1}{\Delta t}\overline{v}^n_j + \mathcal{O}(\lambda),\end{aligned} \tag{107}$$

and expand it making use of (98) and (99)

$$\begin{aligned}\frac{\overline{v}^{n+1}_j - \overline{v}^n_j}{\Delta t} = \Bigg\{&\frac{a^n_{j-\frac{1}{2}}}{2\Delta x}\big(\overline{v}^n_{j-1} + \overline{v}^n_j\big) + \frac{1}{4}a^n_{j-\frac{1}{2}}\big((v_x)^n_{j-1} - (v_x)^n_j\big) \\ &- \frac{1}{2\Delta x}\big[f\big(v^{n+\frac{1}{2}}_{j-\frac{1}{2},r}\big) - f\big(v^{n+\frac{1}{2}}_{j-\frac{1}{2},l}\big)\big] + \frac{1}{2\Delta x}\int_{x^n_{j-\frac{1}{2},l}}^{x^n_{j-\frac{1}{2},r}} S\big(v^{n+\frac{1}{2}}(x),x\big)dx \\ &- \frac{a^n_{j-\frac{1}{2}} + a^n_{j+\frac{1}{2}}}{\Delta x}\overline{v}^n_j + \frac{1}{2}\big(a^n_{j-\frac{1}{2}} + a^n_{j+\frac{1}{2}}\big)(v_x)^n_j\end{aligned}$$

$$
\begin{aligned}
&- \frac{1}{\Delta x}\Big[f\big(v^{n+\frac{1}{2}}_{j+\frac{1}{2},l}\big) - f\big(v^{n+\frac{1}{2}}_{j-\frac{1}{2},r}\big)\Big] + \frac{1}{\Delta x}\int_{x^n_{j-\frac{1}{2},r}}^{x^n_{j+\frac{1}{2},l}} S\big(v^{n+\frac{1}{2}}(x), x\big)dx \\
&+ \frac{a^n_{j-\frac{1}{2}}}{2\Delta x}\big(\overline{v}^n_j + \overline{v}^n_{j+1}\big) + \frac{1}{4}a^n_{j+\frac{1}{2}}\big((v_x)^n_j - (v_x)^n_{j+1}\big) \\
&- \frac{1}{2\Delta x}\Big[f\big(v^{n+\frac{1}{2}}_{j+\frac{1}{2},r}\big) - f\big(v^{n+\frac{1}{2}}_{j+\frac{1}{2},l}\big)\Big] + \frac{1}{2\Delta x}\int_{x^n_{j+\frac{1}{2},l}}^{x^n_{j+\frac{1}{2},r}} S\big(v^{n+\frac{1}{2}}(x), x\big)dx\Bigg\} \\
&+ \mathcal{O}(\lambda). \qquad (108)
\end{aligned}
$$

In the limit $\Delta t \to 0$, the midpoint interface values approach

$$
\begin{aligned}
v^{n+\frac{1}{2}}_{j+\frac{1}{2},r} &\to v_{j+1}(t) - \frac{\Delta x}{2}(v_x)_{j+1}(t) =: v^+_{j+\frac{1}{2}}(t), \\
v^{n+\frac{1}{2}}_{j+\frac{1}{2},l} &\to v_j(t) + \frac{\Delta x}{2}(v_x)_j(t) =: v^-_{j+\frac{1}{2}}(t),
\end{aligned} \qquad (109)
$$

and we obtain (22)–(23)

$$
\begin{aligned}
\frac{d}{dt}\overline{v}^n_j(t) = &- \frac{H_{j+\frac{1}{2}} - H_{j-\frac{1}{2}}}{\Delta x} + \frac{1}{\Delta x}\Bigg[\frac{1}{2}\int_{x^-_{j-\frac{1}{2}}}^{x^+_{j-\frac{1}{2}}} S(v,x)dx + \int_{x^+_{j-\frac{1}{2}}}^{x^-_{j+\frac{1}{2}}} S(v,x)dx \\
&+ \frac{1}{2}\int_{x^-_{j+\frac{1}{2}}}^{x^+_{j+\frac{1}{2}}} S(v,x)dx\Bigg] \qquad (110)
\end{aligned}
$$

with $H_{j\pm\frac{1}{2}}$ given by (19) as desired.

References

1. Abgrall, R., Karni, S.: Two-layer shallow water system: a relaxation approach. SIAM J. Sci. Comput. **31**(3), 1603–1627 (2009). doi:10.1137/06067167X
2. Armi, L.: The hydraulics of two flowing layers with different densities. J. Fluid Mech. **163**, 27–60 (1986)
3. Armi, L., Farmer, D.: Maximal two-layer exchange through a contraction with barotropic net flow. J. Fluid Mech. **186**, 27–51 (1986)
4. Balbás, J., Karni, S.: A central scheme for shallow water flows along channels with irregular geometry. Modél. Math. Anal. Numér. **43**(2), 333–351 (2009). doi:10.1051/m2an:2008050
5. Balbas, J., Tadmor, E.: Nonoscillatory central schemes for one- and two-dimensional magnetohydrodynamics equations. ii: High-order semidiscrete schemes. SIAM J. Sci. Comput. **28**(2), 533–560 (2006). doi:10.1137/040610246. http://link.aip.org/link/?SCE/28/533/1
6. Balbás, J., Tadmor, E., Wu, C.C.: Non-oscillatory central schemes for one- and two-dimensional MHD equations. I. J. Comput. Phys. **201**(1), 261–285 (2004)
7. Castro, M.J., García-Rodríguez, J.A., González-Vida, J.M., Macías, J., Parés, C., Vázquez-Cendón, M.E.: Numerical simulation of two-layer shallow water flows through channels with irregular geometry. J. Comput. Phys. **195**(1), 202–235 (2004)
8. Farmer, D., Armi, L.: Maximal two-layer exchange over a sill and through the combination of a sill and contraction with barotropic flow. J. Fluid Mech. **164**, 53–76 (1986)
9. Gottlieb, S., Shu, C.W., Tadmor, E.: Strong stability-preserving high-order time discretization methods. SIAM Rev. **43**(1), 89–112 (2001) (electronic)

10. Harten, A.: High resolution schemes for hyperbolic conservation laws. J. Comput. Phys. **49**, 357–393 (1983)
11. Jiang, G.S., Levy, D., Lin, C.T., Osher, S., Tadmor, E.: High-resolution nonoscillatory central schemes with nonstaggered grids for hyperbolic conservation laws. SIAM J. Numer. Anal. **35**(6), 2147–2168 (1998) (electronic)
12. Kurganov, A., Levy, D.: A third-order semidiscrete central scheme for conservation laws and convection-diffusion equations. SIAM J. Sci. Comput. **22**(4), 1461–1488 (2000) (electronic)
13. Kurganov, A., Levy, D.: Central-upwind schemes for the Saint-Venant system. Modél. Math. Anal. Numér. **36**(3), 397–425 (2002)
14. Kurganov, A., Noelle, S., Petrova, G.: Semidiscrete central-upwind schemes for hyperbolic conservation laws and Hamilton-Jacobi equations. SIAM J. Sci. Comput. **23**(3), 707–740 (2001) (electronic)
15. Kurganov, A., Petrova, G.: A second-order well-balanced positivity preserving central-upwind scheme for the Saint-Venant system. Commun. Math. Sci. **5**(1), 133–160 (2007)
16. Kurganov, A., Petrova, G.: Central-upwind schemes for two-layer shallow water equations. SIAM J. Sci. Comput. **31**(3), 1742–1773 (2009). doi:10.1137/080719091
17. Kurganov, A., Tadmor, E.: New high-resolution central schemes for nonlinear conservation laws and convection-diffusion equations. J. Comput. Phys. **160**(1), 241–282 (2000)
18. Lax, P.D.: Weak solutions of nonlinear hyperbolic equations and their numerical computation. Commun. Pure Appl. Math. **7**, 159–193 (1954)
19. van Leer, B.: Towards the ultimate conservative difference scheme. V. A second-order sequel to Godunov's method. J. Comput. Phys. **135**(2), 227–248 (1997). J. Comput. Phys. **32**(1), 101–136 (1979)
20. Levy, D., Puppo, G., Russo, G.: A third order central WENO scheme for 2D conservation laws. Appl. Numer. Math. **33**(1–4), 415–421 (2000)
21. Mabe, N.: Steady-state solutions to shallow-water flows along channels with varying geometry. Master's thesis, California State University, Northridge, US (2010)
22. Nessyahu, H., Tadmor, E.: Nonoscillatory central differencing for hyperbolic conservation laws. J. Comput. Phys. **87**(2), 408–463 (1990)
23. Roe, P.L.: Approximate Riemann solvers, parameter vectors, and difference schemes. J. Comput. Phys. **43**(2), 357–372 (1981)
24. Russo, G.: Central schemes for balance laws. In: Hyperbolic problems: theory, numerics, applications, vols. I, II, Magdeburg, 2000. Internat. Ser. Numer. Math., vols. 140, 141, pp. 821–829. Birkhäuser, Basel (2001)
25. Shu, C.W., Osher, S.: Efficient implementation of essentially nonoscillatory shock-capturing schemes. II. J. Comput. Phys. **83**(1), 32–78 (1989)
26. Vázquez-Cendón, M.E.: Improved treatment of source terms in upwind schemes for the shallow water equations in channels with irregular geometry. J. Comput. Phys. **148**(2), 497–526 (1999)
27. Wetzel, A.: Properties of steady-state solutions for shallow water flows. Tech. Rep., University of Michigan, Ann Arbor, Department of Mathematics (2007)
28. Wetzel, A.: Properties of steady-state solutions for critical two-layer shallow water flows. Tech. Rep., University of Michigan, Ann Arbor, Department of Mathematics (2008)